Revisiting the paleomagnetism of the Neoarchean Uauá mafic dyke swarm, Brazil: Implications for Archean supercratons

J. Salminen[a,b,*], E.P. Oliveira[c], E.J. Piispa[d,e], A.V. Smirnov[d,f], R.I.F. Trindade[g]

[a] *Physics Department, University of Helsinki, P.O. Box 64, 00014, Finland*
[b] *Department of Geosciences and Geography, University of Helsinki, P.O. Box 64, 00014, Finland*
[c] *Department of Geology and Natural Resources, Institute of Geosciences, University of Campinas, Campinas 13083-970, Brazil*
[d] *Department of Geological and Mining Engineering and Sciences, Michigan Technological University, Houghton, MI 49931, USA*
[e] *School of Earth Sciences, Energy and Environment, Yachay Tech, Hacienda San Jose s/n y Proyecto Yachay, San Miguel de Urcuqui, Ecuador*
[f] *Department of Physics, Michigan Technological University, Houghton, MI 49931, USA*
[g] *Instituto de Astronomia, Geofísica e Ciências Atmosféricas, Universidade de São Paulo, Rua do Matão, 1226, São Paulo, SP 055080-090, Brazil*

ARTICLE INFO

ABSTRACT

The original connections of Archean cratons are becoming traceable due to an increasing amount of paleomagnetic data and refined magmatic barcodes. The Uauá block of the northern São Francisco craton may represent a fragment of a major Archean craton. Here, we report new paleomagnetic data from the 2.62 Ga Uauá tholeiitic mafic dyke swarm of the Uauá block in the northern São Francisco craton, Eastern Brazil. Our paleomagnetic results confirm the earlier results for these units, but our interpretation differs. We suggest that the obtained characteristic remanent magnetization for the 2.62 Ga swarm is of primary origin, supported by a provisionally-positive baked contact test. The corresponding paleomagnetic pole (25.2°N, 330.5°E, $A_{95} = 8.1°$, N = 20) takes the present northern part of the São Francisco craton to moderate latitudes. Based on the comparison of the paleolatitudes of cratons with high-quality paleomagnetic data and magmatic barcodes, we suggest that the northern part of the São Francisco craton could have been part of the proposed Supervaalbara supercraton during the Archean. Supervaalbara is proposed as including (but not limited to) the part of the São Francisco craton as well as the Superior, Wyoming, Kola + Karelia, Zimbabwe, Kaapvaal, Tanzania, Yilgarn, and Pilbara cratons.

1. Introduction

The Archean–Paleoproterozoic transition (ca. 3.0–2.0 Ga) witnessed fundamental changes across the entire Earth system (Reddy and Evans, 2009; Smirnov et al., 2013). This was reflected in global geodynamics, which transitioned towards modern-style plate tectonics during that interval (Reddy and Evans, 2009; Condie and Kröner, 2013). Most of the preserved Archean cratons show rifted margins of Proterozoic age and are crosscut by numerous regional mafic dyke swarms, indicating that they are fragments of larger ancestral landmasses (Williams et al., 1991) that Bleeker (2003) called supercratons. Bleeker and Ernst (2006) proposed that by comparing the magmatic barcodes of different cratons, the nearest neighbors of once-connected cratons could be found. Bleeker (2003) postulated that supercratons had an Archean stabilized core, which on break-up spawned several independently drifting cratons. He further proposed that based on the cratonization

history, the cratons could be divided into different clans that were connected within a supercraton. Smirnov et al. (2013) additionally proposed that dyke swarms are more diagnostic in defining nearest neighbors than the overall basement geology by pointing out that rift-related dykes can show nearest-neighbor connections even among suture-bounded provinces with different ages (for example, the Central Atlantic Magmatic Province). Moreover, although the comparison of magmatic barcodes aids in finding the nearest neighboring cratons, high-quality paleomagnetic data are needed to study the kinematics. Several recent and ongoing studies combining paleomagnetism and geochronology have produced high-quality Archean and Paleoproterozoic paleomagnetic data. The paleogeography and magmatic barcodes are becoming defined for some of the Archean cratons, such as Superior (in North America), Karelia and Kola (in Scandinavia), Zimbabwe and Kaapvaal (in Southern Africa), and Pilbara and Yilgarn (Western Australia) (e.g. Bleeker, 2003; Bleeker and Ernst, 2006; Mertanen et al.,

2006b; de Kock et al., 2009; Evans and Halls, 2010; Söderlund et al., 2010; Smirnov et al., 2013; Salminen et al., 2014; Pisarevsky et al., 2015; Gumsley et al., 2015, 2016, 2017; Evans et al., 2017).

Due to their similar cratonization history and the matching of two or more coeval 2.5–2.1 Ga dyke swarms, the Superior, Hearne and possibly Wyoming (North American) cratons and the Karelia and Kola (Baltica) cratons have been proposed to exist in tight fit in a long-lived supercraton named Superia (Bleeker and Ernst, 2006; Ernst and Bleeker, 2010). In their Superia fit, Bleeker and Ernst (2006) reconstructed the Northern Karelian craton against the Matachewan dyke swarm in the Southeastern Superior craton. Bleeker and Ernst (2006) did not include paleomagnetic information from the Karelia craton in their model. To date, most of the paleomagnetic data obtained from Karelia (e.g., Mertanen et al., 1999; 2006b; Mertanen and Korhonen, 2011; Salminen et al., 2014) negate the Superia fit with Superior at 2.50–2.45 Ga, but allow a different configuration of these cratons. The paleomagnetic poles of Karelia and Kola support the existence of these cratons in their present-day relative configuration, at least between 2.5 and 2.4 Ga. Based on the coeval (2.58 Ga, 2.47 Ga, 2.41 Ga) generations of dykes within the Sebanga swarm in the Zimbabwe craton and the magmatic events in Superior, Hearne, Kola, and Karelia, Söderlund et al. (2010) suggested that they could have been nearest neighbors during the Archean. Moreover, the Zimbabwe craton has been proposed to form a supercraton, Zimgarn, together with the Western Australian Yilgarn craton (Smirnov et al., 2013). The distinctive 2.41 Ga age match between the Widgiemooltha and Sebanga Poort dykes (Söderlund et al., 2010) may be diagnostic of the original connection of Yilgarn and Zimbabwe, despite the mismatch of the cratonization ages for these cratons (Smirnov et al., 2013; see an alternative reconstruction by Pisarevsky et al., 2015). Smirnov et al. (2013) proposed that the Zimgarn connection could be as early as the cratonization intervals of these continents (2.7–2.6 Ga), lasting until ca. 2.2–2.0 Ga.

Another Southern African craton, Kaapvaal, and a Western Australian craton, Pilbara, have been proposed to form a supercraton, Vaalbara, based on similarities in stratigraphic elements. In particular, good indicators are the Paleoproterozoic iron formations (Trendall, 1968), but there are also broader links between the 3.5 Ga and 1.8 Ga volcano-sedimentary basins and mineral deposits (e.g., Button, 1979; Cheney, 1996). This connection was later supported with paleomagnetic data (de Kock et al., 2009), but invalidated by a more detailed geochronological study on the Kaapvaal craton that demonstrated a mismatch of the magmatic barcodes for the Kaapvaal and Pilbara cratons (Gumsley et al. 2015, 2016, 2017). Gumsley et al. (2017) proposed that the Kaapvaal and Pilbara cratons were not nearest neighbors, but were instead parts of a much larger supercraton. The authors further proposed that this Archean supercraton included Superior, Wyoming, Hearne, Kola + Karelia, Kaapvaal, and Pilbara, and perhaps also the Singhbhum craton of India, because the geological evolution of all these cratons was very similar in the Paleoproterozoic. Gumsley (2017) named it Supervaalbara. The Zimbabwe and Yilgarn cratons could also be parts of Supervaalbara, despite their dissimilar cratonization history (Söderlund et al., 2010; Smirnov et al., 2013; see also Pisarevsky et al., 2015 for a different configuration). Supervaalbara appears geologically distinct from the Rae clan of cratons, suggesting two separate supercratons in the early Paleoproterozoic (Gumsley et al., 2015, 2016, 2017).

South American cratons have been absent from most of the Archean supercraton reconstructions. However, based on sedimentary and magmatic records, Aspler and Chiarenzelli (1998) proposed two separate Neoarchean supercontinents (called supercratons hereinafter). One of the supercratons included the present southern hemisphere cratons (i.e. Zimbabwe, Kaapvaal, Pilbara, Singhbhum, and São Francisco), whereas the other included the present northern hemisphere cratons (i.e. all the cratons of North America, Baltica, and Siberia). In contrast, based on the similar geological history and/or matching coeval dyke swarms of different cratons, we adopt the concept of the Supervaalbara

supercraton (Gumsley et al., 2017), where cratons from the present northern and southern hemispheres could have been parts of the same supercraton. Our goal was to test whether a fragment of the São Francisco craton, the Uauá block, was part of the Neoarchean Supervaalbara supercraton. For this, we have obtained new paleomagnetic data from the 2623.8 ± 7.0 Ma (U-Pb on zircon) tholeiitic dyke and 2726.2 ± 3.2 Ma (U-Pb on baddeleyite) noritic dyke swarms in the Uauá block (Oliveira et al., 2013). Here we use the name *Uauá tholeiite dykes* for the 2.62 Ga tholeiitic dykes, and *norite dykes* for the 2.73 Ga noritic dykes. Eventually, a different name can be chosen for the norite dykes once the swarm is better characterized. The two investigated dyke swarms can be genetically linked to each other by the progressive thinning of the Uauá lithosphere by extension that ultimately may have led to the break-up of the craton and ocean basin formation at ~2624 Ma (Oliveira et al., 2013). The particular geological characteristics of the Uauá block, i.e. shear zone boundaries, the presence of layered complexes and several mafic dyke swarms, that are not found in the adjacent terranes, support a model in which the Uauá block may represent a lost fragment of a major Archean craton (Oliveira et al., 2013).

Paleomagnetism of the Uauá tholeiite dyke swarm has previously been studied by D'Agrella-Filho and Pacca (1998). They sampled three groups of dykes: (1) metamorphosed amphibolites, (2) basic dykes, and (3) metamorphosed basic dykes. Based on field observations, the basic dykes of D'Agrella-Filho and Pacca (1998) correspond to the 2.62 Ga tholeiite dyke swarm of our study with primary igneous texture and minor replacement of pyroxene by hornblende. D'Agrella-Filho and Pacca (1998) found characteristic remanent magnetization directions (ChRMs) with northerly–northeasterly declinations and a steep downward-pointing inclination in all the three groups. Similar directions were also obtained for the host rock baked by the tholeiitic (basic) dykes. Nevertheless, the authors suggested that the ChRM is a secondary remanence acquired during uplift followed by a slow cooling of the crust during the final stages of the Paleoproterozoic Transamazonian cycle. This interpretation was based on available K-Ar and $^{40}Ar/^{39}Ar$ ages spanning the interval of 1.93–2.14 Ga. Rb/Sr mineral isochrons for the tholeiitic dykes suggested two different generations of emplacement, at 2.38 Ga (minimum age) and 1.98 Ga. We sampled ten 2.62 Ga Uauá tholeiite dykes and two 2.73 Ga norite dykes, aiming to obtain additional paleomagnetic data and to test whether the obtained ChRM represents primary remanent magnetization. Here, we present a presumably Neoarchean 2.62 Ga paleomagnetic pole for the Uauá block. Furthermore, a plausible Archean reconstruction is provided based on comparison of the paleomagnetic data, dyke swarms, and matching magmatic barcodes of Archean cratons.

2. Geological setting

The São Francisco (SF) craton is located in the northeastern part of Brazil (Fig. 1a). It is surrounded by Proterozoic to Cambrian orogens, which welded together the supercontinent Gondwana. The basement rocks of the SF craton are dominated by Archean to Paleoproterozoic high-grade migmatite and granulite gneisses, and granite-greenstones (Teixeira et al., 2000; Barbosa and Sabaté, 2004; Heilbron et al., 2017). These rocks are covered by Meso- to Neoproterozoic sedimentary rocks of the Espinhaço Supergroup and the São Francisco Supergroup (Alkmim et al., 1993; Barbosa et al., 2003; Danderfer et al., 2009). The basement of the SF craton is composed of a number of Archean blocks (e.g. the Gavião, Jequié, and Serrinha), a number of Archean greenstone belts, and the Itabuna-Salvador-Curaçá orogen (Barbosa and Sabaté, 2004; Teixeira et al., 2017), which aggregated during the Archean and Proterozoic, mainly during the time interval 2.1–1.8 Ga (Teixeira and Figueiredo, 1991; Teixeira et al., 2017) at the onset of the amalgamation of the Nuna supercontinent.

The studied mafic dykes occur within the Serrinha block, located in the northeastern part of the SF craton (Fig. 1b). The Serrinha block
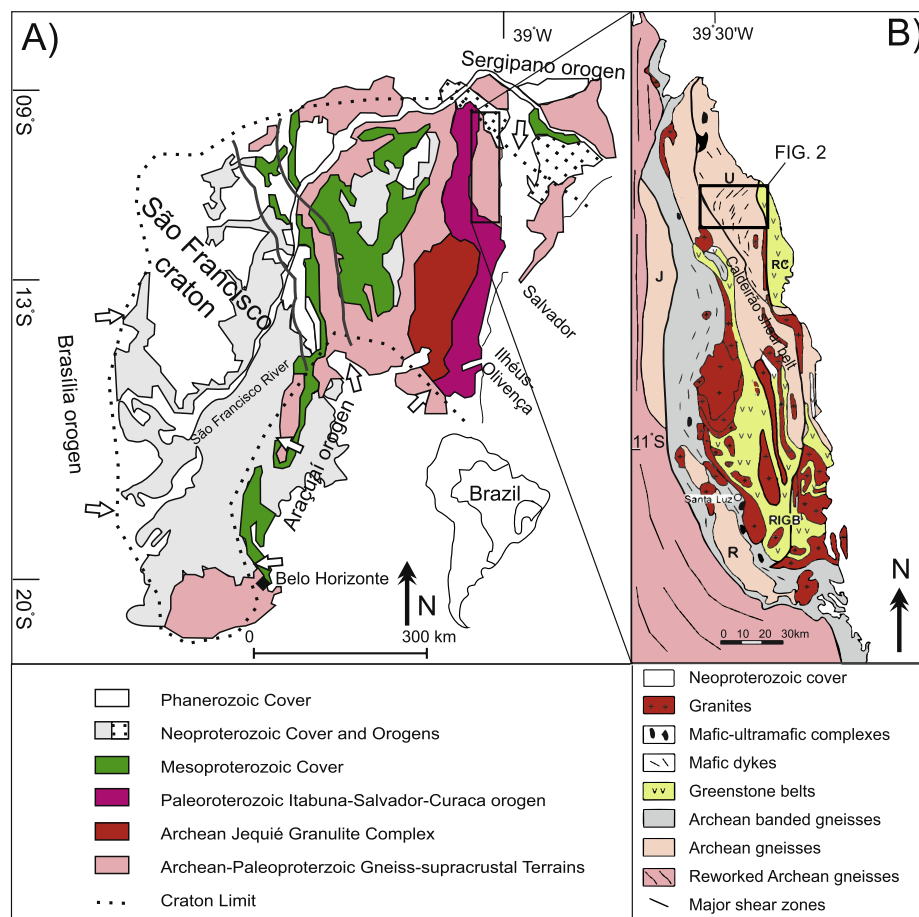
Fig. 1. (a) Simplified geology of the São Francisco craton and (b) the Serrinha block after Oliveira et al. (2013). White arrows in (a) indicate orogenic vergence. J – Jequié, R – Retirolândia, U – Uauá, RIGB – Rio Itapicuru Greenstone Belt, RC –Rio Capim Greenstone Belt.

comprises a basement complex of migmatites, banded gneisses, or-thogneisses, mafic dykes and mafic–ultramafic complexes (Oliveira, 2011). The basement lies in tectonic contact with supracrustal se-quences of the Paleoproterozoic Rio Itapicuru and Rio Capim green-stone belts, and with the Archean-Paleoproterozoic Caldeirão belt. The Serrinha block contains three Mesoarchean (3.15 – 2.93 Ga) basement domains: the Uauá, Jacurici, and Retirolândia gneiss-migmatite com-plexes. The dykes occur within the Uauá block (Fig. 2), which is bor-dered by the Caldeirão shear belt to the west and by the Rio Capim greenstone belt to the east (Oliveira et al., 2011).

The basement of the Uauá block mostly consists of NW-trending banded gneisses intruded by layered anorthosite (Paixão and Oliveira, 1998), peridotite and diorite complexes, and by tonalite-granodiorite bodies (Mascarenhas and Sá, 1982; Cordani et al., 1999; Oliveira et al., 1999). Recently, Oliveira et al. (2015a,b, 2016) reported the occurrence of ca. 3.2–2.9 Ga TTG gneisses, ca. 2.82 Ga high-pressure mafic gran-ulites, and ca. 2.95 Ga sanukitoids in the Uauá block. Most of these rocks were metamorphosed under granulite facies conditions and later retrogressed to amphibolite grade. The Uauá block is intruded by at least three mafic dyke swarms (Bastos Leal et al., 1995; Bellieni et al., 1995; Oliveira et al., 2013): (1) the NW-trending metamorphosed am-phibolite dykes (the oldest swarm), (2) the NW-trending un-metamorphosed noritic dykes, and (3) the NE-trending un-metamorphosed 2.62 Ga Uauá tholeiitic dyke swarm (Bastos Leal et al., 1995; Bellieni et al., 1995; Oliveira, 2011; Oliveira et al., 2013). Oliveira et al. (2013) obtained an age of 2726.2 ± 3.2 Ma (U–Pb on baddeleyite) for a NW-trending noritic dyke, and an age of 2623.8 ± 7.0 Ma (U–Pb on zircon) for a NE-trending Uauá tholeiitic dyke. These ages are consistent with previous less precise whole-rock

Sm-Nd ages of 2744 ± 65 Ma and 2586 ± 66 Ma for noritic and tholeiitic dykes, respectively (Oliveira et al., 1999).

The trend for noritic dykes is variable, with some dykes exhibiting NW, or N directions, and they may belong to several different swarms. Sampled noritic dykes are mainly composed of plagioclase and ortho-pyroxene, and sometimes also olivine, brown amphibole, biotite-phlo-gopite, pyrrhotite, and ilmenite (Oliveira et al., 2013). They preserve a primary igneous texture (Oliveira et al., 2013).

The tholeiitic dykes are the most abundant. Their thickness varies from a few centimeters to several tens of meters. They are occasionally sheared at the margins, but in the center the primary mineralogy (calcic pyroxene, plagioclase and magnetite) and intergranular igneous texture are well preserved (Oliveira et al., 2013). Pyroxene is often replaced by green to brown amphibole at the rim. The trend of tholeiitic dykes is variable (Fig. 2). In the central part of the Uauá block, where we sampled, the dykes are not significantly deformed and the trend is northeast (Fig. 1b). The dykes gradually change direction from NE–SW, through N–S to NW–SE, when they become parallel to the Caldeirão shear belt and finally disappear towards the western margin of the block (Fig. 1b; Oliveira et al., 2013).

3. Sampling and methods

3.1. Sampling

Samples were taken from ten 2.62 Ga Uauá tholeiitic dykes (sites U1, U3, U5, U6, U7, U8, U9, U10A, U10B, and U11) and from two unmetamorphosed 2.73 Ga norite dykes (sites U2 and U4) (Fig. 2). Five to thirteen standard 2.54-cm-diameter cores were collected from each
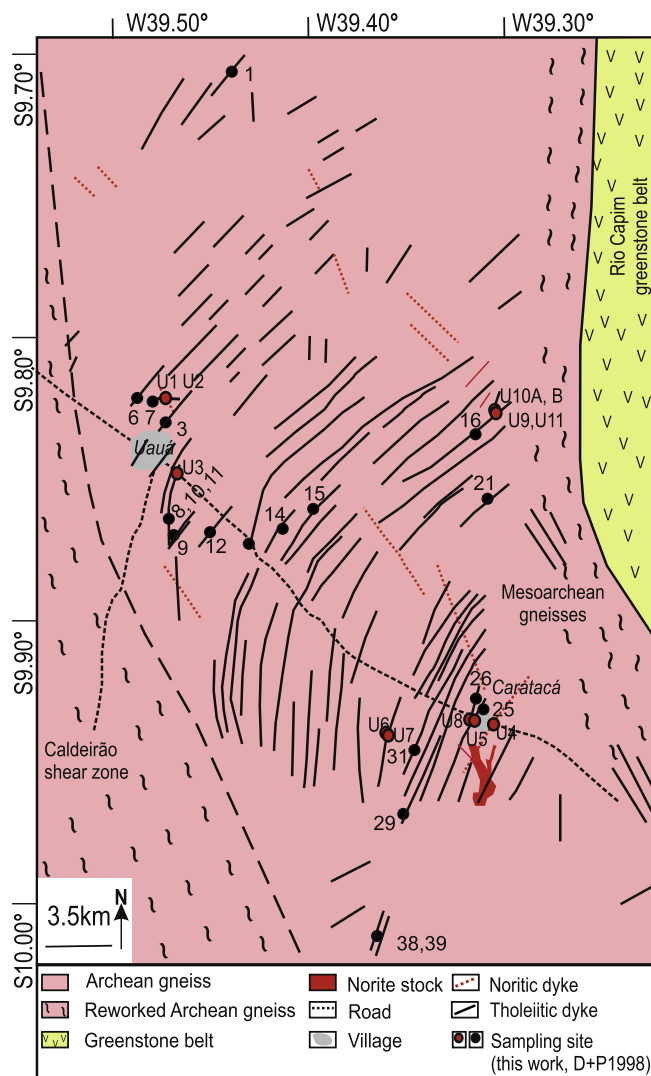
Fig. 2. Geological map with the sampling sites of this work and tholeiitic dykes of D́Agrella-Filho and Pacca (D + P1998) in the Uauá block, São Francisco craton.

dyke with a portable drill (Table 1). The cores were oriented using solar and/or magnetic compasses. Dyke U4 is the geochronology site of Oliveira et al. (2013), yielding an age of 2726.2 ± 3.2 Ma. This dyke is

crosscut by a younger thin tholeiitic dyke (not sampled). Tholeiitic dyke U3 has been dated at 2623.8 ± 7.0 Ma (Oliveira et al., 2013). Tholeiitic dyke 10B cuts tholeiitic dyke 10A. The baked and unbaked host rocks were collected for the 2.62 Ga Uauá tholeiitic dykes at sites U1, U3, U9, and U10A.

3.2. Laboratory methods

All the measurements were conducted in the Solid Earth Geophysics Laboratory at the University of Helsinki, Finland. Room temperature susceptibility was measured with a ZH Instruments magnetic susceptibility meter (SM100) using a frequency of 1026 Hz and a magnetic field of 320 A/m. Density was defined using the Archimedean principle by weighing samples in air and in water. Natural remanent magnetization (NRM) and magnetization after each demagnetization step were measured using a 2G–DC SQUID magnetometer. Stepwise alternating field (AF) demagnetizations were carried out using a three-axis demagnetizer with a maximum field up to 160 mT, coupled with the magnetometer. Sister specimens were stepwise thermally demagnetized using an ASC Scientific TD-48SC furnace with inert argon atmosphere. Both methods were effective and provided stable results. Vector components were isolated using principal component analysis (Kirschvink, 1980) and analyzed with Fisher (1953) statistics, giving a unit weight to each specimen to compute the mean values.

Magnetic mineralogy was investigated by thermomagnetic analysis of selected powdered whole-rock specimens using an Agico KLY-3S-CS Kappabridge system. The samples were cycled to 700 °C in argon gas. Curie temperatures were determined using the Cureval 8.0 program (http://www.agico.com).

4. Results

4.1. Petrophysical results

Petrophysical properties (density, magnetic susceptibility, intensity of natural remanent magnetization (NRM) and Koenigsberger's Q ratio) for the norite and Uauá tholeiite dyke samples are summarized in Table 1. The bivariate diagrams of density versus NRM and susceptibility versus NRM are illustrated in Fig. 3. Koenigsberger's Q ratio is calculated with the field value of 24.7 μT and shown with lines in Fig. 3b (for the equation, see the footnote for Table 1).

Based on their magnetic properties, the Uauá tholeiite dykes form a group (U3, U5, U6, U8, U10A, and U10B) with a few outliers (U1, U7, and U9). All tholeiite dykes except U10B show a coherent density (mean 2888 kg/m³), lower than the density of norite dykes (mean 3012 kg/m³), whereas dyke U10B has a similar density to that of the

Table 1
Site-mean petrophysical properties of the 2.73 Ga norite and 2.62 Ga Uauá tholeiite dyke swarms.

Site	Rock type	Lat(°S)	Long(°E)	N/n	Density(kg/m³)	Susceptibilit(10⁻⁶SI)y	NRM(mA/m)	Q-value
U2	Norite dyke	9.81594	320.52248	7*/10	3044 ± 40	19922 ± 2650	2966 ± 1548	7.6
U4	Norite dyke	9.93285	320.68126	9*/11	2980 ± 98	5799 ± 1320	2748 ± 1367	24.1
U1	Tholeiitic dyke	9.81575	320.52261	9*/13	2850 ± 52	12942 ± 17013	317 ± 232	1.2
U3	Tholeiitic dyke	9.84540	320.53047	8*/11	2930 ± 18	31273 ± 6227	5742 ± 1089	9.3
U5	Tholeiitic dyke	9.93183	320.67246	9*/12	2863 ± 107	14657 ± 2021	6374 ± 3080	22.1
U6	Tholeiitic dyke	9.93940	320.63319	8*/12	2842 ± 82	2911 ± 1358	3118 ± 1057	54.5
U7	Tholeiitic dyke	9.93991	320.63401	6*/8	2925 ± 14	1253 ± 50	249 ± 84	10.1
U8	Tholeiitic dyke	9.93159	320.67145	8*/11	2897 ± 70	15641 ± 4281	5045 ± 3003	16.4
U9	Tholeiitic dyke	9.81530	320.68241	4*/5	2877 ± 16	839 ± 24	3 ± 2	0.2
U10A	Tholeiitic dyke	9.81174	320.67671	7*/9	2908 ± 79	47397 ± 15023	12523 ± 11858	13.4
U10B	Tholeiitic dyke	9.81174	320.67671	2*/2	2996 ± 1	117450 ± 2450	9411 ± 1060	4.1
U11	Tholeiitic dyke	9.81256	320.67709	8*/10	2891 ± 40	10013 ± 4710	8860 ± 6657	45.0

Each site is one dyke (cooling unit). Lat/Long, site latitude and longitude. N/n, number of samples/specimens. * denotes the statistical level used for mean calculations. NRM, the intensity of the natural remanent magnetization. Q, Koenigsberger's ratio was calculated using the equation $Q = \frac{\mu_0 \times NRM}{\chi H}$, where μ_0 is the magnetic permeability of vacuum ($4\pi10^{-7}$ Tm/A) and χ is volume susceptibility in SI units, the magnetic field value of Bahia, Brazil (H = 24.7μT) was used. The uncertainties shown are one standard deviation.
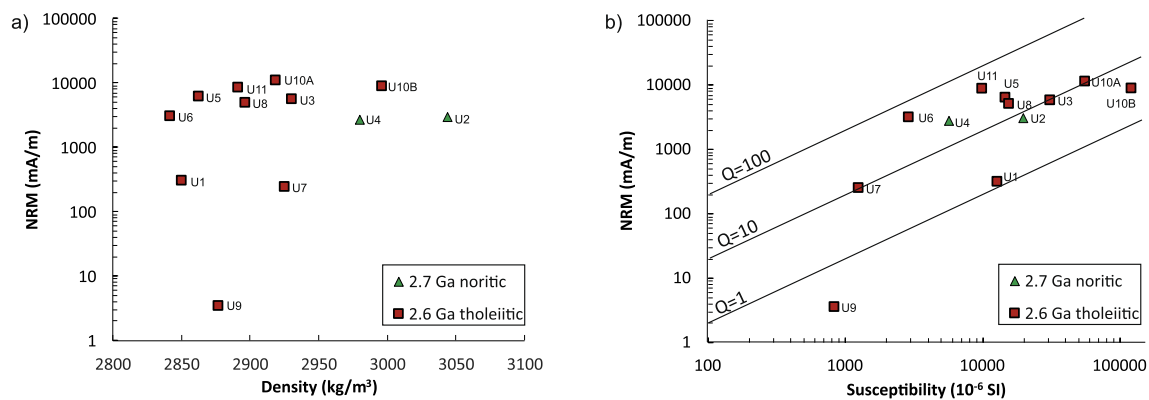
Fig. 3. (a) Natural remanent magnetization (NRM) versus density (semilogarithmic scale) and (b) NRM versus susceptibility (logarithmic scale) diagrams for the 2.62 Ga Uauá tholeiite and 2.73 Ga norite dykes. Koenisgsberger's Q ratios (calculated with the field value of 24.7 μT) are presented as straight lines in (b). Sites are indicated with site codes.
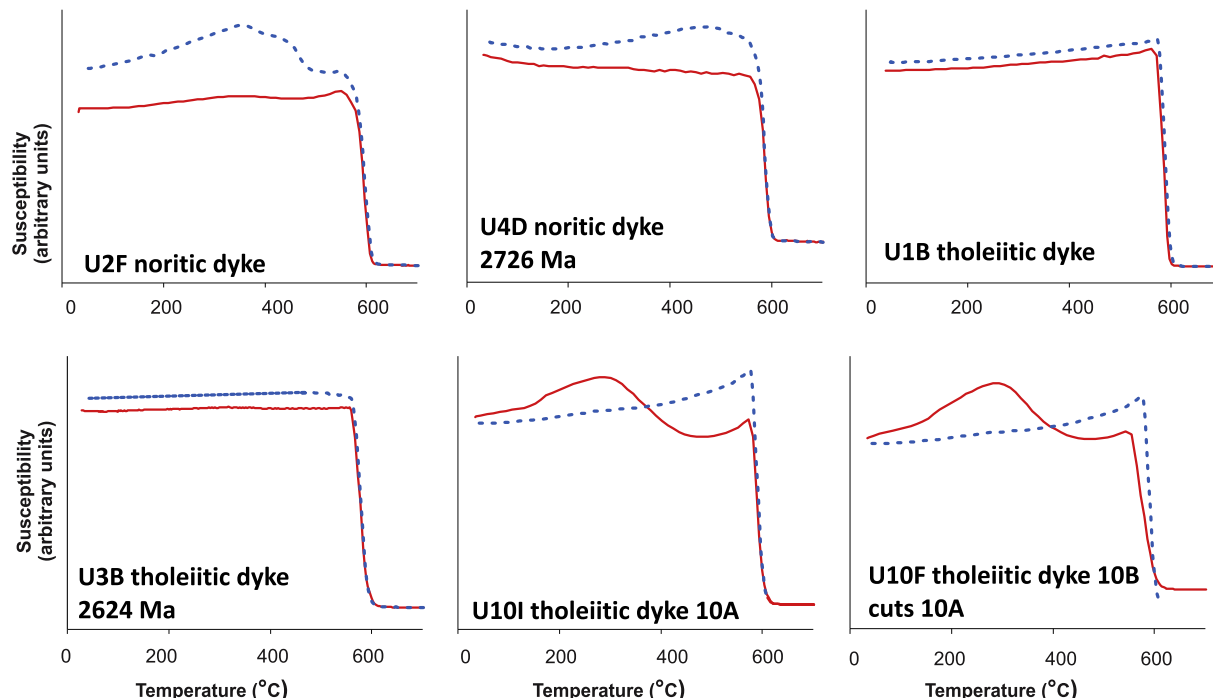

Fig. 4. Low-field thermomagnetic curves for the 2.72 Ga noritic and the 2.62 Ga Uauá tholeiitic dyke samples. The red (solid) line denotes heating and the blue (dashed) line denotes cooling.

norites (Fig. 3a). The main group of Uauá tholeiite dykes displays higher NRM values (range 3000–12 500 mA/m) than the two norite dykes (range 2700–3000 mA/m). However, the NRMs of U1 and U7 are an order of magnitude, and those of dyke U9 - two orders of magnitude lower than the main group values. The susceptibility values are more widely distributed. Uauá tholeiite dykes U7 and U9 show the lowest susceptibility values (ca. 800 × 10⁻⁶ SI), and the main group of tholeiite dykes show values between (14 000–120 000 × 10⁻⁶ SI). The noritic dykes show susceptibility values (6 000–20 000 × 10⁻⁶ SI) similar to the lower range of the main Uauá tholeiite group values.

The Koenigsberger's ratios (Q values) are within 0.2–55 for all the dykes (Table 1). U9 shows the lowest Q value (0.2), indicating the dyke's poor ability to carry remanence. During the paleomagnetic analyses, this dyke displayed the recent field overprint direction. A high Q ratio (higher than 20) sometimes indicates that a strong magnetic field, for example due to lightning strikes, has imprinted on the NRM of the rocks with an isothermal remanent magnetization. However, in the case of lightning strikes, the NRM directions are usually randomized,

which is not the case with the dykes showing higher Q values.

4.2. Magnetic mineralogy

Thermomagnetic (low-field susceptibility versus temperature) curves for both 2.73 Ga norite and 2.62 Ga Uauá tholeiite dykes indicate the presence of magnetite in the samples (Fig. 4), consistent with the paleomagnetic results. Norite samples (U2F and U4D) show irreversible heating and cooling curves (Fig. 4 a,b). The heating curve for norite dyke U4 is a shoulder type with a Curie point of 586C, indicating magnetite. The cooling curve reveals a minor formation of magnetite during heating. The heating curve of norite dyke U2 displays a slight hump in susceptibility around 360 °C representing titanomaghemite. It also shows a characteristic magnetite Curie point of 587 °C and a pronounced Hopkinson's peak, which is a typical feature of stable single-domain/pseudo-single-domain magnetite (Dunlop and Özdemir, 1997). The cooling curve indicates that both new magnetite and titano-magnetite formed during heating.

Table 2

New paleomagnetic results from this study combined with previous results for the 2.62 Ga Uauá tholeiite dyke swarm and 2.73 Ga norite dykes.

Site	Rock type	Trend/Dip	Width(m)	Lat(°N)	Long(°E)	B/N/n	D (°)	I (°)	α95 (°)	k	Plat (°N)	Plong (°E)	Ref	Comment
2.62 Ga Uauá tholeiite dykes														
U1	Tholeiitic dyke	92/90	1	-9.8159	320.5226	0.5/9*/12	010.2	71.9	5.1	73.1	21.7	326.7	1	U1 cuts through U2
U3	Tholeiitic dyke	17/90	20	-9.8454	320.5304	0.5/8*/8	015.2	70.1	2.5	478.0	24.6	330.2	1	2623.8 ± 7.0[a]
U5	Tholeiitic dyke	27/90	10	-9.9318	320.6724	0.5/6*/6	042.2	40.9	11.4	35.6	36.6	010.7	1	
U7	Tholeiitic dyke	12/90	70	-9.9399	320.6340	1/5*/5	024.1	84.0	12.3	39.5	0.1	325.4	1	
U8	Tholeiitic dyke	17/90	30	-9.9315	320.6714	0.5/6*/6	058.1	70.5	12.3	30.8	8.7	349.3	1	
U10A	Tholeiitic dyke	22/90	10	-9.81	320.7009	0.5/3*/3	345.8	77.9	7.9	244.4	12.7	314.9	1	
1	Tholeiitic dyke			-9.7	320.6	1/2*/2	348.5	55.4			43.2	307.7	2	
3	Tholeiitic dyke			-9.8	320.5	1/4*/4	026.6	75.0	8.3	124.0	15.4	333.2	2	
6	Tholeiitic dyke			-9.8	320.5	1/2*/2	038.6	55.2			31.8	357.1	2	
7	Tholeiitic dyke			-9.8	320.5	0.5/3*/3	348.4	65.5	11.2	121.0	31.6	311.3	2	
8	Tholeiitic dyke			-9.8	320.5	0.5/4*/4	008.3	66.6	9.4	96.0	30.6	326.8	2	
9	Tholeiitic dyke			-9.8	320.5	1/3*/3	024.3	69.3	8.3	223.0	23.9	336.2	2	
10	Tholeiitic dyke			-9.8	320.5	1/4*/4	317.4	76.4	17.2	29.0	9.2	303.2	2	
11	Tholeiitic dyke			-9.9	320.5	1/3*/3	025.9	73.2	6.9	318.0	18.2	334.2	2	
12	Tholeiitic dyke			-9.9	320.6	1/3*/3	049.5	73.6	9.8	161.0	10.2	343.6	2	
14	Tholeiitic dyke			-9.8	320.6	1/3*/3	359.6	67.1	13.3	87.0	30.3	320.3	2	
15	Tholeiitic dyke			-9.8	320.6	1/2*/2	036.2	73.5			14.9	338.7	2	
16	Tholeiitic dyke			-9.8	320.7	0.5/1*/1	080.2	57.6			1.5	011.4	2	
21	Tholeiitic dyke			-9.9	320.7	1/3*/3	007.7	71.7	9.5	170.0	23.3	325.3	2	
25	Tholeiitic dyke			-9.9	320.7	0.5/2*/2	002.9	62.9			35.6	323.3	2	
26	Tholeiitic dyke			-9.9	320.7	0.5/3*/3	013.3	71.8	30.8	17.0	22.5	328.5	2	
29	Tholeiitic dyke			-9.9	320.7	1/2*/2	019.3	60.6			35.6	338.3	2	
31	Tholeiitic dyke			-9.9	320.7	1/2*/2	352.4	62.5			35.8	313.9	2	
38	Tholeiitic dyke			-10.0	320.6	1/3*/3	354.6	51.5	7.2	301.0	32.5	313.8	2	
39	Tholeiitic dyke			-10.0	320.6	1/3*/3	017.9	63.6	9.2	180.0	47.8	335.5	2	
MEAN 2.62 Ga Uauá tholeiite dykes						20*/89/92	**015.3**	**68.9**	**5.4**	**37.4**	**25.2**	**330.5**	**1**	**2623.8 ± 7.0[a]**
											A95 = 8.1°	K = 17.3		
MEAN 2.62 Ga Uauá tholeiite dykes[#]						25*/89/92	**017.2**	**68.8**	**5.0**	**34.9**	**25.0**	**331.4**	**1**	**2623.8 ± 7.0[a]**
											A95 = 7.4°	K = 16.4		
Tholeiitic dykes not included in the mean														
U9	Tholeiitic dyke	57/80	2.5	-9.81530	320.68241	3*/3	305.9	-23.1	26.0	23.6	37.1	222.5	1	MDF > 100 mT
U10B	Tholeiitic dyke	?	0.05	-9.81174	320.67671	2*/2	339.9	75.4			15.8	311.6	1	Cuts through dyke U10A
2.73 Ga norite dykes interpreted to be remagnetized by 2.62 Ga Uauá tholeiite dykes														
U2	Norite dyke	157/?	4	-9.81594	320.52248	2/4*	352.3	75.3	12.1	58.8	17.2	317.1	1	Cut by U1, see Table 3
U4	Norite dyke	30/?	50	-9.93285	320.68126	6/6*	039.2	60.4	2.9	536.4	27.3	352.9	1	2726.2 ± 3.2[a]

Trend/Dip, Structural orientation (trend and dip) of dykes. Width, width of dykes. For the sites of D'Agrella-Filho and Pacca (1998), the trend and width information was not available. Lat/Long, site latitude and longitude. For the sites of D'Agrella-Filho and Pacca (1998), the sampling latitude and longitudes were recalculated using declination, inclination, pole latitude, and pole longitude. (B/)N/n, number of (sites/)samples/specimens. * The number used to calculate the mean value. D, declination; I, inclination. α_{95}, the radius of the 95% confidence cone in Fisher (1953) statistics. k, Fisher (1953) precision parameter. Plat/Plong, latitude/longitude of the pole. A$_{95}$, radius of the 95% confidence cone of the pole. K, Fisher (1953) precision parameter of the pole. Ref, 1 – this study, 2 – D'Agrella-Filho and Pacca, 1998 (DP98). MDF, median destructive field. [a], from Oliveira et al. (2013). Based on the recalculated sampling locality and observation of the previous drill holes, our sites U1, U3, U5, U8, and U10A are equivalent to Sites 7, 8, 25, 26, and 16 of DP98, respectively. Sites U2, U4, U7, U9, and U10B were not sampled by DP98. [#] The mean calculated considering each site-mean as an independent field reading.

Uauá tholeiitic dykes U1 and U3 display nearly reversible heating and cooling curves (Fig. 4c,d). Shoulder-type heating curves with Hopkinson's peaks and Curie temperatures of 585 °C (U1) and 580 °C (U3) indicate single-domain/pseudo-single-domain magnetite. Tholeiitic dykes U10A and U10B demonstrate a moderate hump around 295 °C in their heating curves, possibly due to titanomaghemite, a sharp Hopkinson's peak, and a Curie temperature of ca. 583 °C characteristic of magnetite (Fig. 4 e,f). The cooling curve indicates that the phase with lower Curie temperature (titanomaghemite) transforms to magnetite during heating.

4.3. Paleomagnetic results

The paleomagnetic results of our work are presented in Table 2, and representative demagnetization behaviors are illustrated in Figs. 5–7. In Table 2, we also list the previous results of D'Agrella-Filho and Pacca (1998) for the 2.62 Ga Uauá tholeiite dyke swarm, which are discussed later in this chapter.

For our sampled 2.62 Ga Uauá tholeiitie and 2.73 Ga norite dykes, both alternating field (AF) and thermal (TH) treatments were sufficient to separate the characteristic remanent magnetization (ChRM) component (Table 5; Figs. 5-7). Median destructive fields (MDFs) during the AF treatment of these dykes range from 7 to 20 mT, displaying nearly linear trajectories to origin, indicating that no higher coercivity component is present in the samples (Fig. 5). The exception is tholeiitic dyke U9, which shows MDF values of 100 mT and magnetization directions close to the present Earth field (PEF) direction at the sampling site (D = 337°, I = -28°; Fig. 6). TH demagnetization of all the dykes except tholeiitic dykes U9 and U11 indicates unblocking temperatures between 570 °C and 580 °C, demonstrating that magnetite is the main carrier of ChRM. Dykes U9 and U11 show lower unblocking temperatures around 320–400 °C. Tholeiitic dykes U6 and U11 gave inconsistent results between the sampled blocks, but coherent results within the blocks, indicating that the sampled blocks were not *in situ*. The results from these two dykes are not discussed further.

4.3.1. Paleomagnetic results for the 2.62 Ga tholeiitic dykes

The ChRM directions for the five 2.62 Ga Uauá tholeiite dykes (U1,
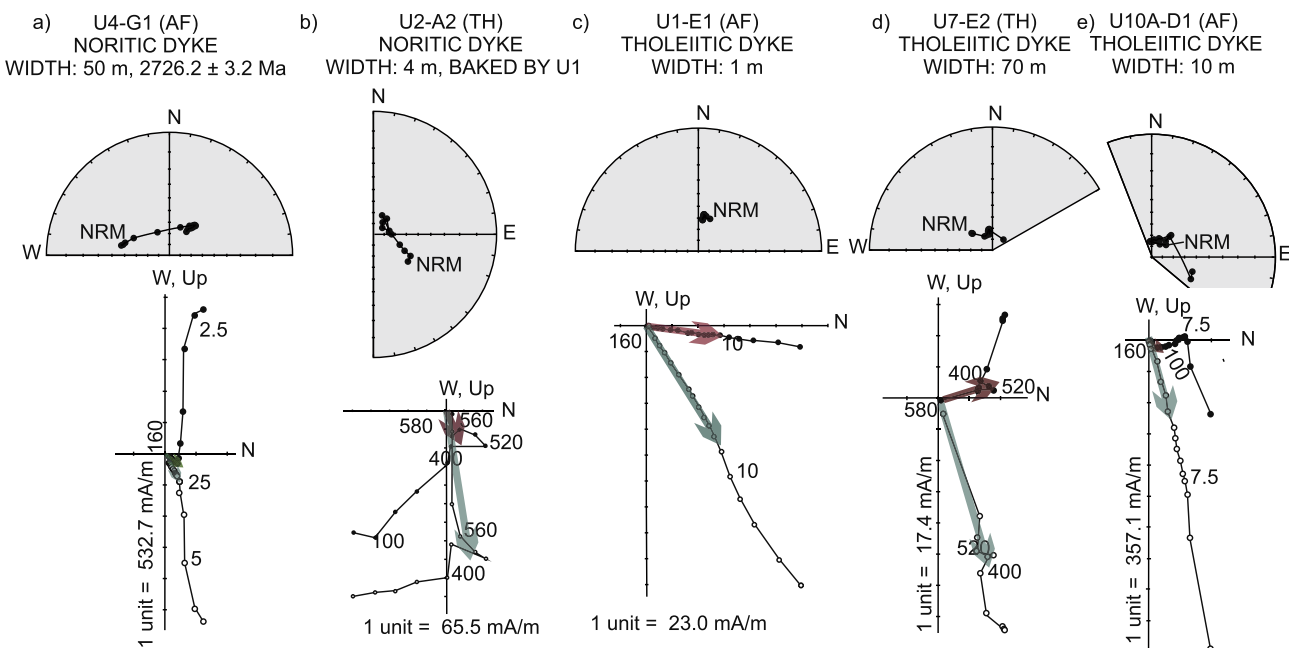
Fig. 5. Representative demagnetization data for the 2.73 Ga norite dykes (a, b) and for the 2.62 Ga Uauá tholeiite dykes (c-e). (a) Dyke U4 (interpreted to be baked by the 2.62 Ga Uauá tholeiitic dykes), (b) Dyke U2 baked by the tholeiite dyke U1, (c) Dyke U1, (d) Dyke U7, and (e) Dyke U10A. On the stereoplots, solid and open symbols represent lower and upper hemisphere vectors, respectively. On the orthogonal projection diagrams, solid symbols show projections onto the horizontal plane, and open symbols show projections onto the vertical plane. The numbers show demagnetization steps in mT (°C) for AF(TH). NRM indicates natural remanent magnetization. The arrows indicate obtained characteristic remanent magnetization direction.
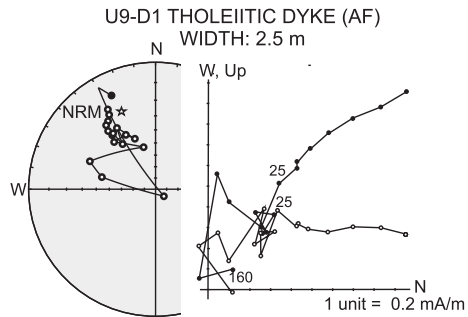
Fig. 6. Representative alternating field demagnetization data for tholeiitic dyke U9, which shows a recently remagnetized direction. Symbols as in Fig. 5. Star indicates the present earth field direction at the sampling site.

U3, U5, U7, and U8) display northerly declinations and steep downward-pointing inclinations, except for dyke U5, which shows intermediate inclinations. Dyke U10A, which is cut by dyke U10B, displays NNW declinations and steep downward-pointing inclinations (Table 2; Fig. 5). The cutting dyke U10B shows similar magnetization direction with U10A. The mean directions were calculated using Fisher statistics (Fisher, 1953). A site mean was accepted for further calculations if it was obtained from three or more samples. We accepted the site means from six 2.62 Ga Uauá tholeiite dykes (U1, U3, U5, U7, U8, and U10A). We combined our results with the previous results of D'Agrella-Filho and Pacca (1998), who accepted one site mean (#16) based on only a single sample, and several site means based on two samples. Most site-means in the prior study (except sites #10 and #26) have α_{95} < 13.3°.

Dyke U9 shows a high coercivity component, with northwesterly declination and intermediate upward-pointing inclination. This direction is similar to that of the present Earth's magnetic field at the sampling site (Fig. 6). A similar direction was obtained for the baked host rock of this site (Table 2). We interpret that the dyke and its baked host rock have recently been remagnetized, and the high coercivity secondary minerals carry a recent overprint magnetization direction. This

interpretation is further supported by the low remanent magnetization values and low Q ratio of this dyke. These results are not discussed further.

4.3.1.1. Baked contact tests for the 2.62 Ga Uauá tholeiite dykes. The baked host rock sample taken directly from the eastern contact of 20-m-wide dyke U3 (the geochronology site of Oliveira et al. (2013)) shows a ChRM similar to that of the dyke (Figs. 7 and 8; Tables 2 and 3). The remanence directions for two unbaked host rock samples taken 20 m east of the dyke have a northerly declination with a shallow upward-pointing inclination, similar to the unbaked host directions measured from sites U9 and 16 (Figs. 7 and 8; Table 3). While the ChRM directions from the baked and unbaked host rocks are well defined (Fig. 7), we interpret these data only as a provisionally-positive full baked contact test due to the small number of samples, which prevents calculating the statistics of mean directions for the baked or unbaked host rocks.

For the tholeiitic Uauá dyke U1, we attempted a baked contact test with both Archean gneiss and cross-cut noritic dyke U2. The baked host rock samples taken directly from the east contact of the 1-m-wide dyke U1 shows ChRMs similar to that of the dyke (Tables 2 and 3). The samples of host gneiss samples taken 7 m east of the dyke yield ChRMs with steep downward inclinations and westerly declinations (Tables 2 and 3, Fig. 8) somewhat resembling the directions from the dyke U1 and baked host rocks. However, we cannot rule out the possibility that these samples were partially remagnetized by another tholeiitic dyke, possibly an offshoot of U1.

The samples of U2 taken within 0.3–2 m from the contact with dyke U1 show northerly declinations and steep downward inclinations, similar to the mean direction of U1 (e.g., Fig. 5b and 8c; Tables 2 and 3). At the same time, the samples of U2 taken at 15–20 m from the dyke U1 did not yield consistent directions (Fig. 8c; Table 3). Because of the small number of samples and the lack of a consistent direction from unbaked rocks, this test cannot be classified as a fully positive and robust baked contact test. However, in opinion, these data can be interpreted as a partial positive baked contact test for U1 against U2.
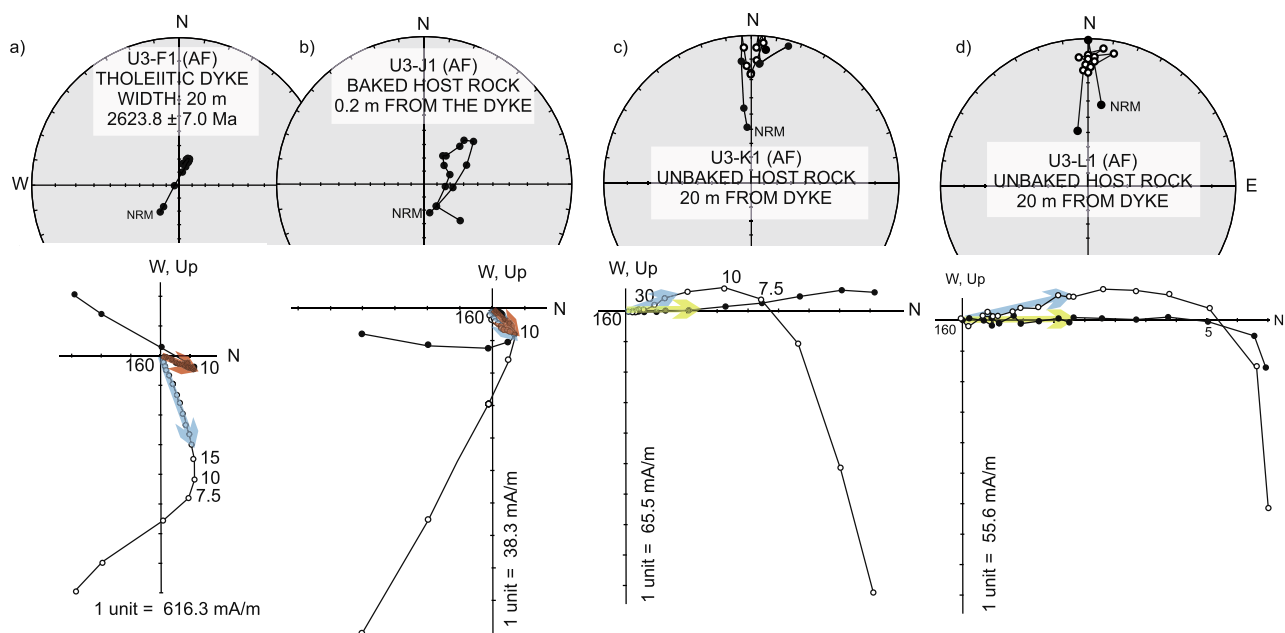
Fig. 7. Provisionally-positive baked contact test for the Uauá tholeiite dyke U3. Representative alternating field demagnetization data for (a) a dyke sample, (b) a baked host rock sample, and (c, d) unbaked host rock samples. Symbols as in Fig. 5.
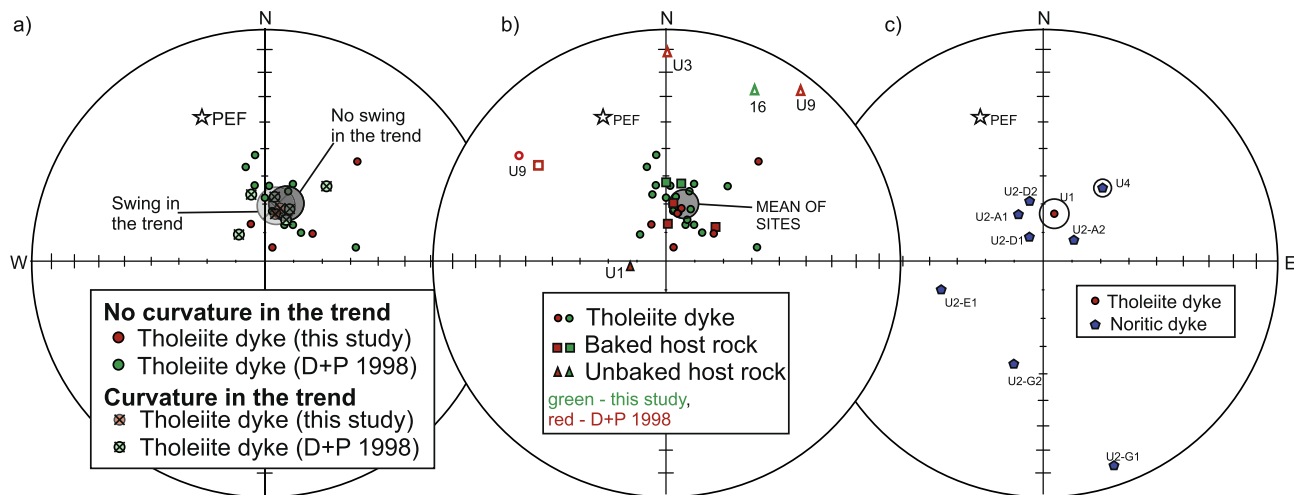

Fig. 8. Paleomagnetic results. (a) The accepted site-mean remanence directions for the Uauá tholeiitic dykes (red symbols – this study; green symbols – D'Agrella-Filho and Pacca, 1998). The Uauá tholeiitic dykes with curvature/swing in the trend are marked with cross (see discussion in the text). The dark grey and light grey crossed circles show the group mean directions with the 95% confidence circle (α_{95}) for the dykes with no curvature and with curvature in the trend, respectively. (b) The mean remanence directions for Uauá tholeiitic dykes, baked host rocks (squares) and unbaked host rock (triangles) samples. The color-coding is the same as in (a). The dark grey circle shows the combined group mean and α_{95} for the Uauá tholeiitic dykes. (c) The site-mean direction for dyke U1 (red circle) with α_{95} that cuts noritic dyke U2, and the sample-level data from the noritic dykes U2 and U4 (pentagons). The samples of U2 (A1-2, D1-2) taken within 0.3–2 m from the contact with dyke U1 show northerly declinations and steep downward inclinations, similar to the mean direction of U1. The samples of U2 (E1, G1-2) taken at 15–20 m from U1 show inconsistent directions. Closed (open) symbols represent downward (upward) directions. The star shows the present Earth field (PEF) direction.

Tholeiitic dyke U9 and its baked host rocks show ChRMs similar to the PEF direction at the sampling site (Fig. 8b), thus indicating a recent overprint. However, the unbaked samples taken at 15 m from the dyke display a northeasterly shallow upward magnetization direction similar to the unbaked samples of sites U3 and 16 (Fig. 8b, Table 3). For site U10, the host rocks did not yield stable ChRM directions. Therefore, for both sites U9 and U10A, the BCTs are inconclusive.

4.3.1.2. Combined paleomagnetic dataset for the 2.62 Ga tholeiite dyke swarm. We combined our results with the earlier results of D'Agrella-Filho and Pacca (1998) for the 2.62 Ga Uauá tholeiitic dykes ("basic dykes"), and used the combined dataset to calculate the mean

magnetization direction (Table 2; Fig. 8b). Baked host rocks for the two sites (#3 and #31) of D'Agrella-Filho and Pacca (1998) show ChRM direction similar to that of the dykes. An unbaked host rock sample for site #16 shows a direction similar to the unbaked host rocks at our sites U3 and U9. These observations provide an additional support to the primary origin of ChRM in the tholeiite dykes.

We cannot exclude the possibility that some of our sites coincide with the sampling locations of D'Agrella-Filho and Pacca (1998). Based on the sampling locality calculated from the paleomagnetic directions and VGPs reported by the authors and on observation of the previous drill holes, we interpret our sites U1, U3, U5, U8, and U10A as equivalent (i.e. representing the same dyke) to Sites 7, 8, 25, 26, and 16

Table 3

Results for baked contact tests for the Uauá tholeiitic dykes.

Site	Trend/Dip	Width(m)	Lat(°N)	Long(°E)	(B/)N/n	D (°)	I (°)	α95 (°)	k	Ref	Comment
Tholeiitic dykes											
U1	92/90	1	-9.8159	320.5226	9*/12	010.2	71.9	5.1	73.1	1	U1 cuts through U2
U3	17/90	20	-9.8454	320.5304	8*/8	015.2	70.1	2.5	478.0	1	
3			-9.8	320.5	4*/4	026.6	75.0	8.3	124.0	2	
16			-9.8	320.7	1*/1	080.2	57.6			2	
31			-9.9	320.7	2*/2	352.4	62.5			2	
U9	57/80	2.5	-9.81530	320.68241	3*/3	305.9	–23.1	26.0	23.6	1	
Baked host rock samples											
U1			-9.81575	320.52261	2*/2	007.7	69.3			1	10 cm from dyke U1
U3			-9.84540	320.53023	1/1	55.5	68.8			1	20 cm dyke U3
3			-9.8	320.5	5*/5	359.8	61.5	17.5	20.0	2	
31			-9.9	320.7	2*/2	009.6	61.3			2	
U9			-9.81530	320.68241	1/1	307.3	–32.0			1	5 cm from dyke U9
Baked noritic dyke samples											
U2-A	157/?	4	-9.81594	320.52248	1/2*	003.5	76.8			1	Within 0.3 – 2 m from the contact with U1
U2-D	157/?	4	-9.81594	320.52248	1/2*	343.4	73.4			1	Within 0.3 – 2 m from the contact with U1
Unbaked noritic dyke samples											
U2-E1	157/?	4	-9.81594	320.52248	1/1	256.1	52.8			1	Within 15 – 20 m from the contact with U1
U2-G1	157/?	4	-9.81594	320.52248	1/1	160.7	9.7			1	Within 15 – 20 m from the contact with U1
U2-G2	157/?	4	-9.81594	320.52248	1/1	196.7	53.7			1	Within 15 – 20 m from the contact with U1
Unbaked host rock											
U1			-9.81575	320.52261	2*/3	258.7	78.2			1	7 m from dyke U1
U3			-9.84540	320.53047	2*/2	000.4	-12.4			1	> 20 m from dyke U3
16			-9.8	320.7	1/1	027.1	-18.8			2	
U9			-9.81530	320.68241	1/1	307.3	–32.0			1	15 m from dyke U9

Trend/Dip, Structural orientation (trend and dip) of dykes. Width, width of dykes. Lat/Long, site latitude and longitude. (B/)N/n, number of (sites/)samples/specimens. * The number used to calculate the mean value. D, declination; I, inclination. α95, the radius of the 95% confidence cone in Fisher (1953) statistics. k, Fisher (1953) precision parameter. Ref, 1 – this study, 2 – D'Agrella-Filho and Pacca, 1998.
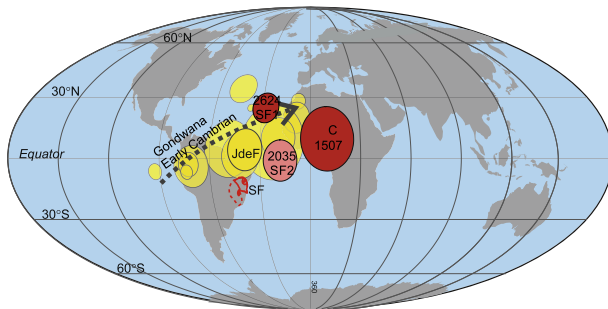
Fig. 9. The new 2.62 Ga paleomagnetic pole for the Uauá tholeiite dykes (SF1) with other poles of the São Francisco craton (red) in the present South American coordinates (Table 4). Pole colors: dark red - a key pole (the rock unit has been adequately dated and the magnetization has proven to be of primary origin) according to key pole criteria of Buchan et al., 2000; Buchan, 2014; pink – a non-key pole; and yellow - paleomagnetic poles of Gondwana (Mitchell et al., 2010). The arrow indicates the progression of ages of the Gondwana poles. Numbers are ages in Ma. Pole abbreviations match those in Table 4. JdeF – pole of Juiz de Fora complex (535–500 Ma, D'Agrella-Filho et al., 2004). The Uauá block and São Francisco craton are outlined with red.

of the prior study, respectively (Table 2). Sites U2, U4, U7, U9, and U10B were not previously sampled. Therefore, the combined dataset represents 20 independently cooled units (dykes). When calculating the group mean direction and paleomagnetic pole, we assigned 0.5 weigh

to each of doubly sampled sites (Table 2). We note that the group means are statistically indistinguishable from the means calculated considering each site-mean as an independent field reading (Table 2) which provides an additional support to the robustness of our analyses.

We interpret the 2.62 Ga dykes as a curvilinear radiating dyke swarm, i.e. the curvature is primary. We are not aware of any literature that would provide unequivocal evidence for the primary nature of the curvature. However, we have conducted a test for possible rotation of paleomagnetic directions by comparing the data from the dykes with curvature (dykes U1, U3, 6–11) with the data from dykes without curvature (shown in Fig. 8a as circles with crosses and plain circles, respectively). The mean directions from these dyke groups (i.e. with and without curvature) are statistically indistinguishable indicating that the curvature does not affect the paleomagnetic direction and, hence, is likely a primary feature. Another indication for the primary nature of the dyke curvature comes from the lack of correlation between the dyke trend and declination although the number of data points is small (we do not have the trends for the sites studied by D'Agrella-Filho and Pacca, 1998). We note however that due to the relatively steep inclinations the potential rotation may be difficult to discern.

4.3.2. Paleomagnetic results for the 2.73 Ga norite dykes

The ChRM directions for the two studied 2.73 Ga norite dykes, U2 and U4, demonstrate northeasterly declinations and steep downward-pointing inclinations, similar to the ChRM of the 2.62 Ga tholeiitic

Table 4

Paleoproterozoic to Mesoproterozoic paleomagnetic poles for the São Francisco craton.

Rock unit	Code	Age (Ma)	Method	PLat (°N)	PLong (°E)	A95(°)	123456 Q(6)	Paleomagnetic reference	Geochronology reference
São Francisco									
Curaçá dykes	C	1506.7 ± 6.9	U-Pb	10	010	15.8	111110 5	Salminen et al. 2016	Silveira et al. 2013
Jequié charnockites	SF2	2035 ± 4	Ar-Ar	-1	342	10.0	011011 4	D'Agrella-Filho et al. 2011	D'Agrella-Filho et al. 2011
Uauà tholeiitic dykes	SF1	2623.8 ± 7.0	U-Pb	25	331	8.1	111110 5	This work	Oliveira et al. 2013

Code, Code used in Fig. 9. Method, Radiometric method used for age determination. PLat, PLong, Latitude and Longitude of the pole. A95, Fisher's (1953) confidence cone radius. 1–6 and Q(6), Reliability criteria from Van der Voo (1990) excluding criterion #7.
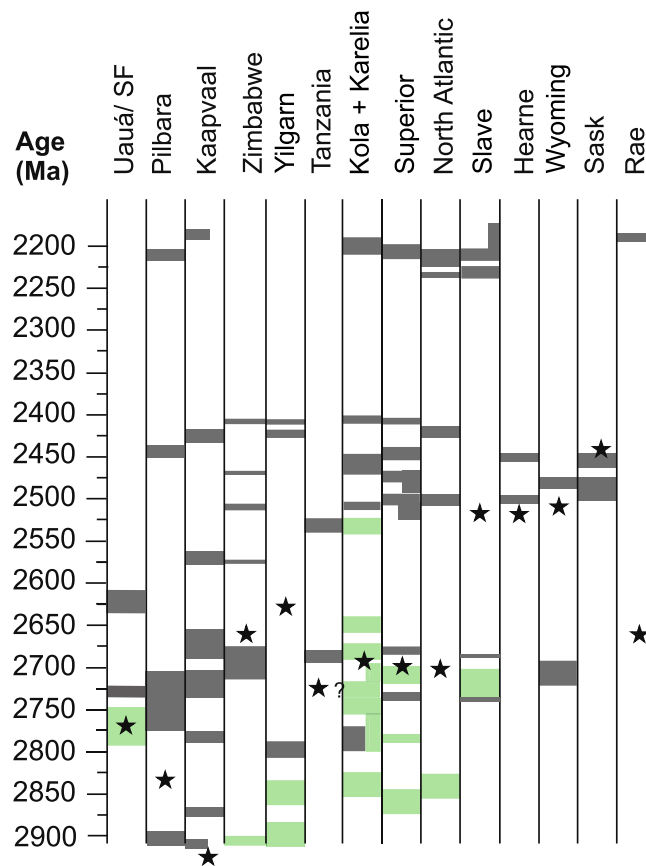
Fig. 10. Barcode record of Archean cratons with mafic intrusions (dyke swarms, sill provinces, and other components of LIPs). Star denotes the end of cratonization (Bleeker, 2003; Van Kranendonk et al., 2012; Halla, et al., 2017). Greenstone belts are indicated with green. The width of individual bars corresponds to the 2σ error in radiometric ages. Uauá block/São Francisco craton: Cordani et al., 1999; Oliveira et al., 1999, 2002, 2011, 2013; Paixão and Oliveira, 1998; Ernst and Buchan, 2001). Pilbara and Kaapvaal cratons: Gumsley et al., 2015, 2016, 2017. Zimbabwe craton: Söderlund et al., 2010. Kola + Karelia cratons: Ernst and Buchan, 2001; Söderlund et al., 2010. Yilgarn craton: Smirnov et al., 2013. Tanzania craton: Meert et al., 1994, 2016; Ernst and Buchan, 2001 and references therein. Superior, Wyoming, Hearne, Slave, North Atlantic, Sask, and Rae: Bleeker et al., 1999; Ernst and Buchan, 2001 and references therein; Ernst and Bleeker, 2010.

dykes (Fig. 5; Tables 2 and 3). We propose that the 2.62 Ga Uauá tholeiite dykes, which are the most abundant dykes in the Uauá block, have completely overprinted the 2.73 Ga norite dykes, and the original remanence of these dykes has not been preserved. The partial positive BCT on U1 against U2 (Section 4.3.1.1) is consistent with this observation (Fig. 3). We also note that, near site U4, we observed an outcrop of tholeiitic dyke that could have re-magnetized U4. Unfortunately, at that location, we could not find any tholeiitic rocks suitable for paleomagnetic sampling.

5. Discussion and conclusions

5.1. The new 2.62 Ga Neoarchean paleomagnetic pole for the Uauá block of the São Francisco craton

The combined dataset of twenty separate 2.62 Ga Uauá tholeiite sites yielded a group mean direction of D = 015.3° and I = 68.9° (α_{95} = 5.4°, k = 37.4) (Fig. 8b). The corresponding paleomagnetic pole is located at Plat = 025.2°N, Plong: 330.5°E (A_{95} = 8.1°, K = 17.3) (Fig. 9). The new pole does not overlap with the other Early and Middle Paleoproterozoic poles for the São Francisco craton (Fig. 9; Table 4).

The pole is ~30° from the Paleoproterozoic 2.0 Ga pole for Jequié charnockites (D'Agrella-Filho et al., 2011) and ~40° from the Mesoproterozoic high-quality 1.5 Ga Curaçá pole (Salminen et al., 2016). Unfortunately, there are no other Archean poles for the São Francisco craton that the new pole can be compared with. We note that the A_{95} for the 2.62 Ga Uauá pole overlaps with the Early-Middle Cambrian poles (ca. 510 Ma) from across Gondwana (McElhinny et al., 2003; Trindade et al., 2004; Mitchell et al., 2010), but not with the Juiz de Fora 535–500 Ma pole (D´Agrella-Filho et al., 2004).

Three "Brasiliano" mountain belts surround the São Francisco craton: the Brasilia belt to the west, the Araçuai belt to the east, and the Riacho do Pontal-Sergipano belt to the north. In all of them, peak metamorphic conditions were attained before 550 Ma (Brito Neves et al., 1999; Oliveira et al., 2010), but remagnetization by low-temperature hydrothermal fluids in the cratonic foreland may have persisted well into the Early Cambrian (Trindade et al., 2004). Nevertheless, the provisionally-positive baked contact test supports the original nature for the ChRM of the 2.62 Ga Uauá tholeiite dykes.

D'Agrella-Filho and Pacca (1998) suggested a secondary origin for the ChRM of the 2.62 Ga dykes acquired during uplift followed by a slow cooling of the crust during the final stages of the Transamazonian cycle. Their interpretation was mainly based on the comparison of their pole with the 2.0 Ga and 1.8 Ga poles of Kalahari in its present-day configuration relative to the Congo craton and the available K-Ar, $^{40}Ar/^{39}Ar$, and Rb/Sr geochronology. However, there is no evidence that Kalahari and Congo were in their present-day configuration in the Archean. Instead, it has been shown that the Kalahari cratons (e.g., Kaapvaal and Zimbabwe) have a distinct drift history in the Archean and Early Paleoproterozoic (e.g., de Kock et al., 2009; Smirnov et al., 2013). This implies that the Kalahari poles cannot be used to determine ages for poles from the São Francisco craton. D'Agrella-Filho and Pacca (1998) pointed out that AF and thermal demagnetization suggested the presence of additional distinct magnetization components with higher coercivities and/or blocking temperatures for 2.62 Ga Uauá tholeiitic dykes. The dykes sampled by us and accepted for the mean calculation showed no indication of higher coercivity or higher/lower unblocking temperature components. Moreover, based on the obtained provisionally-positive baked contact test, we propose that the pole for Uauá tholeiite dykes represents a magnetization age close to its U-Pb age of 2.62 Ga.

5.2. Implications for Archean supercratons

5.2.1. Magmatic age barcode comparison

Age barcodes provide a convenient graphical representation of the magmatic events within cratons. If two or more cratons show coeval magmatic events and tectonic settings at a certain time, it is likely that they were nearest neighbors in an ancestral supercraton (Bleeker and Ernst, 2006). Smirnov et al. (2013) proposed that the cratonization time will not necessarily match between nearest neighbors if they became close to each other after cratonization. Smirnov et al. (2013) further pointed out that dyke swarms are more diagnostic in defining nearest neighbors than the basement geology. Magmatic age barcodes for the northern part of the São Francisco craton (Ernst and Buchan, 2001) were compared with age barcodes for the Pilbara, Kaapvaal, Zimbabwe, Yilgarn, Tanzania, Kola + Karelia, Superior, North Atlantic, Slave, Hearne, Wyoming, Sask, and Rae cratons (data mostly from Ernst and Buchan, 2001) (Fig. 10).

For these cratons, there are three distinct groups based on the cratonization ages. The Uauá block and the Pilbara and Kaapvaal cratons were first to cratonize in the Mesoarchean. The Uauá block appears to have cratonized shortly after the high-pressure granulite facies metamorphism ca 2.82 Ga (Oliveira et al., 2015) and before emplacement of the 2.726 Ga noritic dykes. Cratonization of the Pilbara craton can be assigned to about 2.825–2.800 Ga, after which the 2.772 Ga Black Range mafic dykes emplaced (Wingate, 1999) and the 2.78–2.63 Ga
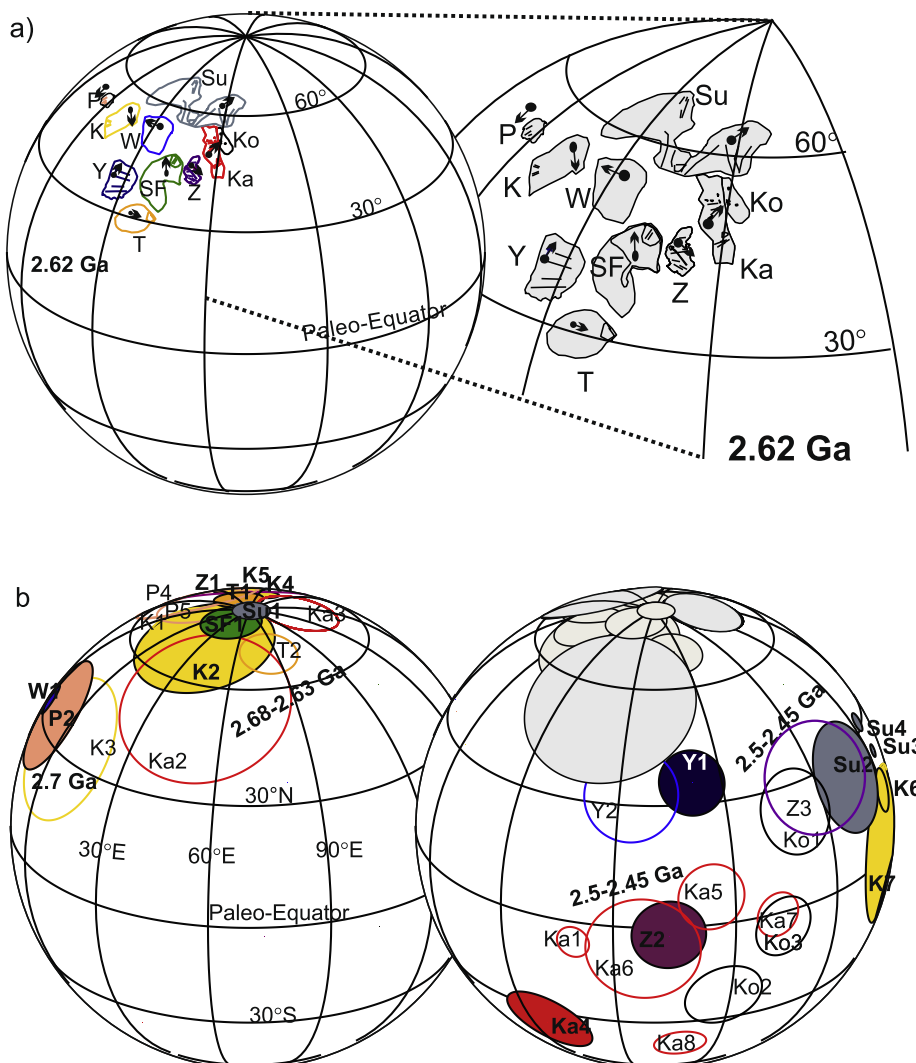
Fig. 11. A plausible global paleogeographic reconstruction at 2.62 Ga. Paleopole numbers are as in Table 5. The bold text and a solid pole with a black outline indicates a key pole (well-defined rock age and proven primary magnetization direction, Buchan 2014). Black arrows indicate the present North. K – Kaapvaal, Ka – Karelia, Ko – Kola, P – Pilbara, Su – Superior, SF -São Francisco, T – Tanzania, W – Wyoming, Y – Yilgarn, Z – Zimbabwe. The used poles are listed in Table 5 and the used Euler rotations are listed in Table 6.

Fortescue Basin developed (Hickman, 2012). Cratonization of the Kaapvaal craton ended by 2.91 Ga (the 3.0–2.8 Ga epicontinental Pongola group). The final stages of cratonization for the Zimbabwe, Yilgarn, Tanzania (?), Kola + Karelia, Superior, North Atlantic and Rae cratons commenced by 2.68–2.63 Ga (Bleeker, 2003; Van Kranendonk et al., 2012; Halla et al., 2017) and were completed in the Neoarchean. The cratonization of Slave, Wyoming, Hearne, and Sask cratons ended in the Paleoproterozoic by 2.53–2.45 Ga (Bleeker, 2003; Van Kranendonk et al., 2012; Halla et al., 2017).

The Kola + Karelia (Kostomuksha), Superior (Crow), North Atlantic (Fiskenaesset), and Yilgarn (Marda) cratons share coeval greenstone belts (with komatiites) of ca. 2.85 Ga in age (Fig. 10). Ca. 2.75–2.80 Ga greenstone belts (with komatiites) coeval with the Rio das Velhas Greenstone Belt (São Francisco) exist in Kola + Karelia (Kuhmo, Ilomantsi, and Olenegorsk) and Superior (Pickle).

Ca. 2.73 Ga magmatism coeval with the noritic dykes exist in the stabilized Pilbara (the Fortescue group) and Kaapvaal (the Ventersdorp group) cratons, and in the non-stabilized Kola + Karelia (Ilomantsi, Kuhmo), Superior (Wabigoon tholeiitic dykes), and Slave (the Kam group) cratons (Fig. 10). The Stillwater complex in Wyoming represents slightly younger magmatism. No magmatism coeval to the 2.62 Ga Uauá tholeiite dyke swarm have been observed for other cratons. The

next magmatic age barcode match for the SF craton is at ca. 2.1 Ga (the Paraopeba tholeiitic dyke swarm) with Kola + Karelia (Karelian mafic dykes), Superior (Marathon mafic dykes), and Wyoming (e.g., Bear Mountain mafic dykes).

Based on similar Mesoarchean cratonization ages and matching 2.73 Ga magmatism, we propose that Uauá, Kaapvaal, and Pilbara were nearest neighbors in the Mesoarchean. Furthermore, based on matching coeval greenstone belt and cratonization ages of Zimbabwe, Yilgarn, Kola + Karelia, Superior, and North Atlantic, we propose that these cratons were nearest neighbors in the Neoarchean. Based on coeval ca. 2.77–2.65 Ga *Sanukitoid granitoids* (Halla et al., 2017) in Karelia, North Atlantic, Superior, Yilgarn, and Kaapvaal/the Limpopo Belt, we propose that these cratons were parts of the same supercraton at this time. Matching 2.73 Ga magmatism adds the Pilbara and Slave cratons to this supercraton.

5.2.2. Reconstructing Archean supercratons

We illustrate a plausible Archean reconstruction of the 2.62 Ga paleogeography in Fig. 11. The paleomagnetic poles and Euler parameters used in the reconstruction are listed in Tables 5 and 6, respectively. We only used the highest quality paleomagnetic data. The Van der Voo (1990) reliability criteria are listed in the Table 5. If the pole fulfils

Table 5
Selected high-quality Archean to Paleoproterozoic global paleomagnetic poles.

Code	Rock unit	Age (Ma)	Method	Age references	Plat (°)	Plon(°)	A95	Q1	Q2	Q3	Q4	Q5	Q6	Q7	Σ	Pole reference
	SÁO FRANCISCO (SF)															
SF1	2.62 Ga Uauà tholeiite dyke swarm	2623.8 ± 7.0	U-Pb (bd)	Oliveira et al. 2013	25.0	331.4	7.4	1	1	1	1	1	0	0	5	This work
SF2	Jequié charnockites	2035 ± 4 (hornblende); 1876 ± 4Ma (biotite)	Ar-Ar	D'Agrella-Filho et al. 2011	-00.5	342.1	9.6	0	1	1	0	1	1	0	4	D'Agrella-Filho et al. 2011
	ZIMBABWE (Z)															
Z1	Belingwe komatiites/Reliance middle temp	2692 ± 9	Pb-Pb	Chauvel et al. 1993	-44.0	302.0	17.0	1	0	1	1	1	0	0	4	Yoshihara and Hamano 2004
Z2	Great dyke Mean	2574 ± 2	U-Pb (bd)	Wingate 2000	24.0	056.0	9.0	1	1	1	1	1	0	1	6	Jones et al. 1975; Smirnov et al. 2013
Z3	Sebanga Poort Dyke (VGP)	2408 ± 2	U-Pb (bd)	Söderlund et al., 2010	17	006	14	1	0	0	1	1	0	0	3	Mushayandebvu et al. 1994
	TANZANIA (T)															
T1	Nyanzian lavas	2680 ± 10	Ar-Ar	Meert et al. 1994	-14.0	330.0	5.9	1	1	1	1	1	1	0	6	Meert et al. 1994
T2	Kisii series	2531 ± 2	U-Pb (zr)	Pinna et al. 2000	-7.0	347.0	8.0	1	1	1	0	1	1	0	5	Brock et al. 1972; Meert et al. 2016
	KAAPVAAL (K)															
K1	Modipe gabbro	2784 ± 1	U-Pb (bd)	Denyszyn et al. 2013	-47.6	012.4	8.6	1	1	1	0	1	1	0	5	Evans and McElhinny, 1966; Denyszyn et al. 2013
K2	Derdepoort basalt	2782 ± 5	U-Pb (zr)	Wingate 1998	-39.6	004.7	17.5	1	1	1	1	1	1	0	6	Wingate, 1998
K3	Westonaria basalt	2714 ± 8	U-Pb (zr)	Armstrong et al. 1991	-17.1	047.9	18.5	1	0	1	0	1	0	0	3	Strik et al. 2007
K4	Allanridge basalts combined	2685 ± ?	U-Pb	Armstrong et al.1991	-69.8	345.6	6.0	1	1	1	1	1	0	0	5	de Kock et al. 2009
K5	Rykoppies dykes	2683 ± 2	U-Pb (bd)	Olsson et al. 2010	-62.1	336.0	3.8	1	1	1	1	1	1	1	7	Lubnina et al. 2010
K6	Ongeluk lavas	2426 ± 3	U-Pb	Gumsley et al. 2017	04.1	282.9	5.3	1	1	1	1	1	0	1	6	Gumsley et al. 2017
K7	Westerberg sill suite	2441 ± 6; 2426 ± 1	U-Pb (bd)	Kampmann et al. 2015	11.8	271.1	19.5	1	0	1	1	1	0	1	5	Kampmann et al. 2015
	WESTERN AUSTRALIAN CRATONS															
	YILGARN (Y)															
Y1	Widgiemooltha dyke suite	2410 ± 3; 2410.3 ± 2.1	U-Pb (bd)	Nemchin and Pidgeon 1998; French et al. 2002	-10.2	159.2	7.5	1	1	1	1	1	1	1	7	Smirnov et al. 2013
Y2	Erayinia mafic dykes	2401 ± 1	U-Pb (bd)	Pisarevsky et al. 2015	-22.7	150.5	11.4	1	1	0	0	1	0	0	4	Pisarevsky et al. 2015
	PILBARA (P)															
P1	Mount Roe Basalts	2772 ± 2	U-Pb (zr)	Wingate 1999	-52.4	178.0	7.6	1	1	1	1	1	1	1	7	Schmidt and Embleton, 1985
P2	Black Range dolerite dykes	2772 ± 2; 2769 ± 1; 2764 ± 3; 2772 ± 2	Pb-Pb; U-Pb (bd)	Wingate 1999; Evans et al. 2017	-03.8	130.4	15.0	1	1	1	1	1	0	1	6	Evans et al. 2017
P3	Pilbara flood basalts package 1	2771 ± 7	APWP	Arndt et al. 1991	41.0	160.0	3.7	1	1	1	1	1	0	1	6	Strik et al. 2003
P4	Pilbara flood basalts package 2	2766 ± 2	U-Pb (zr)	Pidgeon 1984	-46.5	152.7	15.2	1	0	1	0	1	0	0	3	Strik et al. 2003; Blake et al. 2004
P5	Pilbara flood basalts package 4–7	2720–2740	U-Pb (zr)	Blake et al. 2004	-50.4	138.2	12.5	1	1	1	0	1	0	0	4	Strik et al. 2003; Blake et al. 2004
P6	Pilbara flood basalts package 8–10	2710–2721	U-Pb (zr)	Blake et al. 2004	-59.1	186.3	6.1	1	1	1	0	1	1	1	5	Strik et al. 2003
	BALTICA CRATONS															
	KARELIA (Ka)															
Ka1	Panozero sanukitoids	2765 ± 8; 2741 ± 12; 2787.1 ± 4.1	U-Pb	Sergeyev et al. 2007	-10.2	226.1	4.1	1	1	0	0	1	0	1	5	Lubnina and Slabunov 2009
Ka2	Koitere sanukitoids	2684 ± 2	Pb-Pb (monazite)	Halla 2002	-67.5	192.5	21.5	1	1	1	0	1	0	1	5	Mertanen and Korhonen 2011
Ka3	Varpaisjärvi granulite	2630	U-Pb (zr)	Mänttäri and Hölttä 2002	-67.4	154.1	10.0	0	1	0	0	1	0	1	3	Mertanen et al. 2006a
Ka4	Shalskiy thick gabbronorite dyke	2510.6 ± 1.5	U-Pb	Bleeker 2008	22.7	222.1	11.5	1	0	1	1	1	0	1	5	Mertanen et al. 2006b
Ka5	Burakovka intrusion central block	2449 ± 1	U-Pb (zr)	Amelin et al. 1995	-27.6	260.0	8.2	1	0	0	1	1	0	0	3	Fedotova et al. 1999
Ka6	Avdeeb gabbronorite & thin Shalskiy diabase dykes	2449 ± 1	U-Pb (zr)	Amelin et al. 1995	-12.3	243.5	14.0	0	1	1	1	1	0	0	4	Mertanen et al. 2006b
Ka7	Russian Karelia mafic dykes	2446 ± 5	U-Pb (bd)	Vuollo and Huhma 2005	-19.9	278.7	5.7	1	1	0	0	1	0	1	5	Mertanen et al. 1999
Ka8	Taivalkoski 2.3Ga dyke	2339 ± 18	U-Pb (bd)	Salminen et al. 2014	20.4	257.3	6.3	1	1	0	1	1	0	1	4	Salminen et al. 2014
	KOLA (Ko)															
Ko1	Mt. Generalskaya layered Intrusion	2505 ± 1.5	U-Pb (zr bd)	Amelin et al. 1995	-42.5	292.7	10.4	1	1	0	1	1	1	0	5	Arestova et al. 2002
Ko2	Monchegorsk intrusion	2504.4 ± 1.5; 2493 ± 7	U-Pb (zr bd)	Amelin et al. 1995; Balashov et al. 1993	01.3	265.3	9.9	1	1	0	0	0	1	0	4	Pechersky et al. 2004
Ko3	Imandra layered intrusion	2437 ± 11; 2446 ± 39	U-Pb (zr)	Balashov et al. 1993; Bayanova 2004	-16.1	280.3	7.8	1	1	0	1	1	1	1	6	Arestova et al. 2002
	LAURENTIAN CRATONS															
	SUPERIOR (Su)															

Table 5 (*continued*)

Code	Rock unit	Age (Ma)	Age references	Method	Plat (°)	Plong(°)	A95	Q1	Q2	Q3	Q4	Q5	Q6	Q7	Σ	Pole reference
Su1	Otto Stock lamprophyre dykes (eastern reference frame)	< 2680 ± 1	Buchan et al. 1990	Correlation	69.0	227.0	4.8	1	1	1	1	1	1	0	6	Pullaiah and Irving 1975; Buchan et al. 1990; Evans and Halls 2010
Su2	Ptarmigan-Mistassini	2505 ± 2	Buchan et al. 1998	U-Pb (zr bd)	−45.3	213.0	13.8	1	0	1	0	1	0	1	4	Fahrig et al. 1986 Buchan et al. 1998; Evans and Halls 2010
Su3	Matachewan R (rotated across Kapuskasing Structural zone eastern reference frame)	2473 – 2446	Heaman 1997; Halls et al. 2005	U-Pb (zr bd)	−44.1	238.3	1.6	1	1	1	1	1	1	0	6	Evans and Halls 2010
Su4	Matachewan N (rotated across Kapuskasing Structural zone v)	2446 ± 3	Heaman 1997; Halls et al. 2005	U-Pb (zr bd)	−52.3	239.5	2.4	1	1	1	1	1	0	1	6	Evans and Halls 2010
Su5	Nipissing N1	2217 ± 4	Andrews et al. 1986; Noble and Lightfoot 1992	U-Pb (bd)	−17.0	272.0	10	1	1	1	1	1	1	1	7	Buchan et al. 2000
Su6	Senneterre dykes	2216 + 8/4	Buchan et al. 1993	U-Pb (bd)	−15.3	284.3	6.0	1	1	1	1	1	1	1	7	Buchan et al. 1993
	WYOMING (W)															
W1	Stillwater complex	2705 ± 4; 2701 ± 8	De Paolo and Wasserburg 1979; Premo et al. 2000	U-Pb (zr bd)	−83.6	335.8	4.0	1	1	1	1	1	0	0	5	Selkin et al. 2008

Code, corresponds to the code in Fig. 11. Plat Plong, pole latitude and longitude. A95, 95% confidence circle of the pole. Q, Van der Voo (van der Voo 1990) reliability criteria. 1 (0) indicates that the pole fulfils (fails) the criteria. If the pole fulfils criterion Q1 (well defined geochronology) and criterion Q4 (primary magnetization proved by field tests) and some other criteria, it can be called a key pole (Buchan 2014). For Superior, Wyoming, Kola, and Karelia, the north poles are used.

criterion Q1 (well-defined geochronology) and criterion Q4 (primary magnetization proven by a field test) and some other criteria, it can be called a key pole (Buchan, 2014). We use the matching cratonization and magmatic barcodes to propose that northern São Francisco (Uauá), Superior, Karelia + Kola, Zimbabwe, Yilgarn, Tanzania, Kaapvaal and Pilbara were nearest neighbors at 2.62 Ga. Gumsley et al. (2017) proposed an Archean supercraton that included Superior, Wyoming, Hearne, Kola + Karelia, Kaapvaal, and Pilbara. Later, Gumsley (2017) named it Supervaalbara. We follow these authors and call our proposed reconstructed supercraton Supervaalbara.

Superior is reconstructed using the loosely dated Otto Stock pole (Pullaiah and Irving, 1975; Buchan et al., 1990; Evans and Halls, 2010). This pole takes Superior to a high latitude of ca. 60°. Kola is reconstructed to Karelia in its present-day configuration, which is supported by 2.5–2.45 Ga paleomagnetic poles (however, for a different timing of collision, see also Lahtinen et al., 2008; Bogdanova et al., 2008). Karelia + Kola are reconstructed to Superior, distinct from the Superia fit (Bleeker and Ernst, 2006), so that northern Kola is reconstructed to the 2.5 Ga Ptarmigan-Mistassini swarm in eastern Superior, and the Ptarmigan-Mistassini dykes radiate towards 2.5 Ga layered intrusions in Kola. This fit is supported by the 2.63 Ga pole for Karelia (Varpaisjärvi granulites; Mänttäri and Hölttä, 2002; Mertanen et al., 2006a). This fit differs from the Superia fit in which northern Karelia was reconstructed against the 2.45–2.49 Ga Matachewan swarm in Superior. In our Superior – Karelia + Kola fit, the 2.5 Ga pole of Superior overlaps with 2.5–2.45 Ga poles of Kola, which overlap with coeval Karelian poles, thus supporting the proposed reconstruction until 2.5–2.4 Ga.

Zimbabwe and Yilgarn are shown close to the Zimgarn reconstruction (Smirnov et al., 2013). Based on barcode matching, Söderlund et al. (2010) proposed that Zimbabwe and Kola + Karelia were nearest neighbors at 2.4 Ga. Comparison of the 2.7–2.6 Ga poles of Superior, Karelia, and Zimbabwe indicates that Zimbabwe reached the proximity of Karelia between 2.7 Ga and 2.63 Ga. Following Söderlund et al (2010), we reconstructed Zimbabwe close to Karelia so that the orientations of the 2.4 Ga dyke swarms in both cratons (the Sebanga Poort dykes in Zimbabwe and the Taivalkoski dykes in Karelia) match. The 2408.3 ± 2.0 Ma age of the Sebanga Poort Dyke (Söderlund et al., 2010) can be linked to the 2408 ± 2 Ma du Chef swarm in the east Superior craton (Krogh, 1994). Age equivalents in the Kola + Karelia block are represented by the 2403 ± 3 Ma Ringvassøy dykes of northern Kola (Kullerud et al., 2006) and by the 2407 ± 35 Ma Taivalkoski dykes (Vuollo and Huhma, 2005) in northern Karelia. Coeval mafic dyke swarms in Yilgarn are the 2410 ± 3 Ma Widgiemooltha swarm (Nemchin and Pidgeon, 1998; French et al., 2002) and the 2401 ± 1 Ma Erayinia swarm (Pisarevsky et al., 2015). The 2.5–2.45 Ga paleomagnetic poles for Karelia, Kola, Zimbabwe, and Yilgarn support this reconstruction. After 2.45 Ga, the poles of Superior and Karelia + Kola diverge, indicating that rifting and separation of these cratons had started.

Kaapvaal and Pilbara are reconstructed close to Superior, following Gumsley et al. (2017), but using a different rotation, so that the present SW part of the Kaapvaal craton is reconstructed against the present SW part of the Superior craton. In this reconstruction, the 2.4 Ga Ongeluk magmatism (Gumsley et al., 2017) could radiate from the same source as the 2.48–2.45 Ga Matachewan dykes of Superior. We reconstructed Wyoming according to Kilian et al. (2015) close to Superior and Kaapvaal at 2.7 Ga. The 2.7 Ga poles for Kaapvaal, Pilbara, and Wyoming match in this configuration. At 2.5–2.45 Ga, the poles of Kaapvaal and Superior overlap, indicating that this configuration could be valid until the Paleoproterozoic. There are no coeval paleomagnetic poles for Pilbara or Wyoming to test their Paleoproterozoic reconstruction.

The new tentative 2.62 Ga Uauá pole takes the northern part of the São Francisco block to intermediate latitudes of ca. 45° (Fig. 11). Because of the matching cratonization time, greenstone belts, and coeval

Table 6

Euler rotation parameters (E_{lat}° E_{long}° E_{rot}°) for Archean reconstructions shown in Fig. 11.

Craton	Elat (°)	Elong (°)	Rot (°)	Comment
Superior absolute rotation	-76.15	6.53	-100.17	Su1 (Table 5)
Wyoming to Superior	48.00	-95.00	125.00	Kilian et al., 2015
São Francisco absolute rotation	51.53	-68.04	105.60	SF1 (Table 5)
Kola to Karelia	0.00	0.00	304.00	Kola to Karelia in present-day configuration
Karelia	-113.98	-93.60	191.00	Ka3 (Table 5)
Tanzania absolute rotation	13.09	49.85	259.19	Interpolating T1 and T2 (Table 5)
Zimbabwe absolute rotation	-6.56	-121.73	126.56	Interpolating Z1 and Z2 (Table 5)
Yilgarn to Zimbabwe	-45.42	83.69	152.86	Modified Zimgarn (Smirnov et al., 2013)
Kaapvaal absolute rotation	13.87	33.51	-152.01	Interpolating K1 and K5 (Table 5)
Pilbara absolute rotation	7.31	58.01	-206.97	

magmatism at 2.72 Ga, we reconstruct the SF close to the Zimbabwe, Yilgarn, Kola + Karelia, Superior, Kaapvaal, and Pilbara cratons. The matching 2.72 Ga magmatism also supports the close proximity with the Karelia + Kola, Superior, and Wyoming cratons. We propose a reconstruction at 2.62 Ga where the São Francisco craton is between the Wyoming and Zimbabwe cratons, so that the present northern part of the São Francisco craton is pointing towards the present southwestern part of the Wyoming craton. There are no paleomagnetic data to test the life cycle of the northern part of the SF craton in this reconstruction.

Our speculative Archean reconstruction based on a modest amount of paleomagnetic data and comparison of magmatic barcodes demonstrates that the Uauá block could have been part of the Supervaalbara supercraton. Due to the limited amount of Archean–Paleoproterozoic paleomagnetic data for the São Francisco craton, we are currently unable to test the duration of this configuration more precisely. Based on matching paleomagnetic poles and/or magmatic barcodes, we propose that Supervaalbara formed by 2.62 Ga. Mafic magmatism and paleomagnetic data indicate that it started to break up after 2.5–2.45 Ga. The Zimgarn, Kaapvaal, Pilbara, and Superior-Karelia + Kola cratons are thought to have broken off at the latest between 2.2 and 2.0 Ga (Bleeker, 2003; de Kock et al., 2009; Smirnov et al., 2013) and amalgamated by the Paleoproterozoic to form composite cratons (e.g., Laurentia, Baltica, Kalahari, São Francisco).

References

Alkmim, F.F., Brito Neves, B.B., Alves, J.A.C., 1993. Arcabouço tectônico do Cráton do São Francisco — uma revisão. In: Dominguez, J.M.L., Misi, A. (Eds.), O Cráton do São Francisco. Sociedade Brasileira de Geologia, Salvador, pp. 45–62.

Amelin, Yu.V., Heaman, L.M., Semenov, V.S., 1995. U-Pb geochronology of layered mafic intrusions in the eastern Baltic Shield - Implications for the timing and duration of Paleoproterozoic continental rifting. Precambr. Res. 75, 31–46.

Andrews, A.J., Masliwec, A., Morris, W.A., Owsiacki, L., York, D., 1986. The silver deposits at Cobalt and Gowganda, Ontario, II. An experiment in age determinations employing radiometric and paleomagnetic measurements. Can. J. Earth Sci. 23, 1507–1518.

Arestova, N.A., Khramov, A.N., Gooskova, E.G., Iosifidi, A.G., 2002. New paleomagnetic evidence from the Early Proterozoic (2.5-2.4 Ga) Mount Generalskaya and Imandra

layered intrusions, Kola Peninsula. Fizika Zemli 38, 65–76.

Armstrong, R.A., Compston, W., Retief, E.A., Williams, I.S., Welke, H.J., 1991. Zircon ion microprobe studies bearing on the age and evolution of the Witwatersrand Triad. Precambr. Res. 53, 243–266.

Arndt, N.T., Nelson, D.R., Compston, W., Trendall, A.F., Thorne, A.M., 1991. The age of the Fortescue Group, Hamersley Basin, Western Australia, from ion microprobe zircon U-Pb results. Aust. J. Earth Sci. 38, 261–281.

Aspler, L.B., Chiarenzelli, J.R., 1998. Two Neoarchean supercontinents? Evidence from the Paleoproterozoic. Sed. Geol. 120, 75–104.

Balashov, Y.A., Bayanova, T.B., Mitrofanov, F.P., 1993. Isotope data on the age and genesis of layered basic-ultrabasic intrusions in the Kola Peninsula and northern Karelia, northeastern Baltic Shield. Precambr. Res. 64, 197–205.

Barbosa, J.S.F., Sabaté, P., 2004. Archean and Paleoproterozoic crust of the São Francisco Craton, Bahia, Brazil: geodynamic features. Precambr. Res. 133, 1–27.

Barbosa, J.S.F., Sabaté, P., Marinho, M.M., 2003. O Cráton do São Francisco na Bahia: Uma Síntese. Revista Brasileira de Geociências 31, 3–6.

Bastos Leal, L.R., Teixeira, W., Bellieni, G., Petrini, R., Piccirilo, E.M., 1995. Geocronologia e geoquímica isotópica de Sr e Nd nos diques máficos do Curaçá Craton do São Francisco (Brasil): registro de um evento distensivo Neoproterozóico associado à evolução da Faixa Colisional Sergipana. Geochimica Brasiliensis 9 (2), 141–159.

Bayanova, T.B., 2004. Age of reference geological complexes of the Kola region and the duration of igneous processes (in Russian). Nauka, Saint Petersburg, pp. 174.

Bellieni, G., Piccirillo, E.M., Petrini, R., Girardi, V.A.V., Menezes Leal, A.B., Teixeira, W., Bastos Leal, L.R., De Min, A., Comin Chiaramonti, P., Tanner de Oliveira, M.A.F., 1995. Petrological and Sn-Nd evidence bearing on Early Proterozoic magmatic events of the subcontinental mantle: São Francisco craton (Uaua, NE-Brazil). Contrib. Mineralogy Petrol. 122, 252–261.

Blake, T.S., Buick, R., Brown, S.J.A., Barley, M.E., 2004. Geochronology of a Late Archaean flood basalt province in the Pilbara Craton, Australia: constraints on basin evolution, volcanic and sedimentary accumulation, and continental drift rates. Precambr. Res. 133, 143–173.

Bleeker, W., 2003. The late Archean record: a puzzle in ca. 35 pieces. Lithos 71, 99–134.

Bleeker, W., 2008. The pulse of the Earth. Abstract presented at the 33rd International Geological Congress, Oulu, Finland, 6-14 Aug 2008.

Bleeker, W., Ernst, R., 2006. Short-lived mantle generated magmatic events and their dyke swarms: the key unlocking Earth's paleogeographic record back to 2.6 Ga. In: Hanski, E., Mertanen, S., Rämö, T., Vuollo, J. (Eds.), Dyke Swarms - Time Markers of Crustal Evolution. Taylor and Francis/Balkema, London, pp. 3–26.

Bleeker, W., Ketchum, J.W.F., Davis, W.J., 1999. The Central Slave Basement Complex, Part II: age and tectonic significance of high-strain zones along the basement-cover contact. Can. J. Earth Sci. 36, 1111–1130.

Bogdanova, S.V., Bingen, B., Gorbatschev, R., Kheraskova, T.N., Kozlov, V.I., Puchkov, V.N., Volozh, Yu.A., 2008. The East European Craton (Baltica) before and during the assembly of Rodinia. Precambr. Res. 160, 23–45.

Brito Neves, B., Campos Neto, M.C., Fuck, R.A., 1999. From Rodinia to Western Gondwana: an approach to the Brasiliano-Pan African cycle and orogenic collage. Episodes 22, 155–166.

Brock, A., Raja, P.K.S., Vise, J.B., 1972. The palaeomagnetism of the Kisii Series, western Kenya. Geophys. J. R. Astron. Soc. 28, 129–137.

Buchan, K.L., Neilson, D.J., Hale, C.J., 1990. Relative age of Otto stock and Matachewan dykes from paleomagnetism and implications for the Precambrian polar wander path. Can. J. Earth Sci. 27, 915–922.

Buchan, K.L., Mortensen, J.K., Card, K.D., 1993. Northeast-trending Early Proterozoic dykes of southern Superior Province: multiple episodes of emplacement recognized from integrated paleomagnetism and U-Pb geochronology. Can. J. Earth Sci. 30, 1286–1296.

Buchan, K.L., Mortensen, J.K., Card, K.D., Percival, J.A., 1998. Paleomagnetism and U-Pb geochronology of diabase dyke swarms of Minto block, Superior Province, Quebec, Canada. Can. J. Earth Sci. 35, 1054–1069.

Buchan, K.L., Mertanen, S., Park, R.G., Pesonen, L.J., Elming, S.-Å., Abrahamsen, N., Bylund, G., 2000. Comparing the drift of Laurentia and Baltica in the Proterozoic: the importance of key palaeomagnetic poles. Tectonophysics 319, 167–198.

Buchan, K.L., 2014. Reprint of "Key paleomagnetic poles and their use in Proterozoic continent and supercontinent reconstructions: a review". Precambr. Res. 244, 5–22.

Button, A., 1979. Transvaal and Hamersley Basins—review of basin development and mineral deposits. Minerals Sci. Eng. 8, 262–290.

Chauvel, C., Dupré, B., Todt, W., Arndt, N.T., 1993. Pd and Nd isotopic correlation in Belingwe komatiites and basalts. In: Bickle, M.J., Nisbet, E.G. (Eds.) The Geology of the Belingwe Greenstone Belt, Zimbabwe: A Study of the Evolution of Archaean Continental Crust. Geol. Soc. Zimbabwe Spec. Pub. 2, Rotterdam, Balkema, pp. 167–174.

Cheney, E.S., 1996. Sequence stratigraphy and plate tectonic significance of the Transvaal succession of southern Africa and its equivalent in Western Australia. Precambr. Res. 79, 3–24. https://doi.org/10.1016/0301-9268(95)00085-2.

Condie, K., Kröner, A., 2013. The building blocks of continental crust: evidence for a major change in the tectonic setting of continental growth at the end of the Archean. Gondwana Res. 23, 394–402.

Cordani, U.G., Sato K., Nutman A., 1999. Single zircon SHRIMP determination from Archean tonalitic rocks near Uauá, Bahia, Brazil. In: Proceedings II South American Symposium on Isotope Geology, Cordoba, pp. 27–30.

Danderfer, A., De Waele, B., Pedreira, A.J., Nalini, H.A., 2009. New geochronological constraints on the geological evolution of Espinhaço basin within the São Francisco Craton — Brazil. Precambr. Res. 170, 116–128.

D'Agrella-Filho, M.S., Pacca, I.G., 1998. Paleomagnetism of Paleoproterozoic mafic dyke swarm from the Uauá region, northeastern São Francisco Craton, Brazil: tectonic implications. J. S. Am. Earth Sci. 11, 23–33.

D'Agrella-Filho, M.S., Raposo, M.I.B., Egydio-Silva, M., 2004. Paleomagnetic study of the Juiz de Fora complex, SE Brazil: Implications for Gondwana. Gondwana Res. 7, 103–113.

D'Agrella-Filho, M.S., Trindade, R.I.F., Tohver, E., Janikian, L., Teixeira, W., Hall, C., 2011. Paleomagnetism and 40Ar/39Ar geochronology of the high-grade metamorphic rocks of the Jequié block, São Francisco Craton: Atlantica, Ur and beyond. Precambr. Res. 185, 183–201.

de Kock, M.O., Evans, D.A.D., Beukes, N.J., 2009. Validating the existence of Vaalbara in the Neoarchean. Precambr. Res. 174, 145–154.

Denyszyn, S.W., Feinberg, J.M., Renne, P.R., Scott, G.R., 2013. Revisiting the age and paleomagnetism of the Modipe Gabbro of South Africa. Precambr. Res. 238, 176–185.

De Paolo, D.J., Wasserburg, G.J., 1979. Sm-Nd age of the Stillwater complex and the mantle evolution curve for neodymium. Geochim. Cosmochim. Acta 43, 999–1008.

Dunlop, D.J., Özdemir, Ö., 1997. Rock magnetism, fundamentals and frontiers. Cambridge University Press, Cambridge, England, pp. 573.

Ernst, R.E., Buchan, K.L., 2001. Large mafic magmatic events through time and links to mantle plume-heads. In: Ernst, R.E., Buchan, K.L., (eds.) Mantle Plumes: Their Identification Through Time, Geological Society of America Special Paper, 352, pp. 483–575.

Ernst, R.E., Bleeker, W., 2010. Large igneous provinces (LIPs), giant dyke swarms, and mantle plumes: significance for breakup events within Canada and adjacent regions from 2.5 Ga to present. Can. J. Earth Sci. 47, 695–739. https://doi.org/10.1139/E10-025.

Evans, D.A.D., Halls, H.C., 2010. Restoring Proterozoic deformation within the Superior craton. Precambr. Res. 183, 474–489.

Evans, D.A.D., Smirnov, A.V., Gumsley, A.P., 2017. Paleomagnetism and U-Pb geochronology of the Black Range dykes, Pilbara Craton, Western Australia: a Neoarchean crossing of the polar circle. Aust. J. Earth Sci. 64, 225–237.

Evans, M.E., McElhinny, M.W., 1966. The paleomagnetism of the Modipe gabbro. J. Geophys. Res. 71, 6053–6063.

Fahrig, W.F., Christie, K.W., Chown, E.H., Janes, D., Machado, N., 1986. The tectonic significance of some basic dyke swarms in the Canadian Superior Province with special reference to the geochemistry and paleomagnetism of the Mistassini swarm, Quebec, Canada. Can. J. Earth Sci. 23, 238–253.

Fedotova, M.A., Khramov, A.N., Pisakin, B.N., Priyatkin, A.A., 1999. Early Proterozoic palaeomagnetism: new results from the intrusives and related rocks of the Karelian, Belomorian and Kola provinces, eastern Fennoscandian Shield. Geophys. J. Int. 137, 691–712.

Fisher, R., 1953. Dispersion of a sphere. Proc. R. Soc. Lond. 217, 295–305.

French, J.E., Heaman, L.M., Chacko, T., 2002. Feasibility of chemical U-Th-total Pb baddeleyite dating by electron microprobe. Chem. Geol. 188, 85–104.

Gumsley, A., Olsson, J., Söderlund, U., de Kock, M., Hofmann, A., Klausen, M., 2015. Precise U-Pb baddeleyite age dating of the Usushwana Complex, southern Africa – Implications for the Mesoarchaean magmatic and sedimentological evolution of the Pongola Supergroup, Kaapvaal Craton. Precambr. Res. 267, 174–185.

Gumsley, A., Rådman, J., Söderlund, U., Klausen, M., 2016. U-Pb baddeleyite geochronology and geochemistry of the White Mfolozi Dyke Swarm: unravelling the complexities of 2.70–2.66 Ga dyke swarms across the eastern Kaapvaal Craton, South Africa. Geologiska Föreningen 138, 115–132. https://doi.org/10.1080/11035897.2015.1122665.

Gumsley, A.P., 2017. Validating the existence of the supercraton Vaalbara in the Mesoarchaean to Palaeoproterozoic. Doctoral dissertation, Lithosphere and Biosphere Science, Department of Geology, Lund University. Litholund theses 30, 130.

Gumsley, A.P., Chamberlain, K.R., Bleeker, W., Söderlund, U., de Kock, M.O., Larsson, E.R., Bekker, A., 2017. Timing and tempo of the Great Oxidation Event. PNAS 114, 1811–1816. https://doi.org/10.1073/pnas.1608824114.

Halla, J., 2002. Origin and Paleoproterozoic reactivation of Neoarchean high-K granitoid rocks in eastern Finland. Finnish Academy of Science and Letters. Annales Academiae Scientiarum Fennicae, Geologica-Geographica 163, 105.

Halla, J., Whitehouse, M.J., Ahmad, T., Bagai, Z., 2017. Archaean granitoids: an overview and significance from a tectonic perspective. In: Halla, J., Whitehouse, M. J., Ahmad, T., Bagai, Z. (eds). Crust–Mantle Interactions and Granitoid Diversification: Insights from Archaean Cratons. Geological Society, London, Special Publications, 449, pp. 1–18.

Halls, H.C., Stott, G.M., Davis, D.W., 2005. Paleomagnetism, Geochronology and Geochemistry of Several Proterozoic Mafic Dike Swarms in Northwestern Ontario.

Ontario Geological Survey Open File Report 6171, 59.

Heaman, L.M., 1997. Global mafic magmatism at 2.45 Ga: remnants of an ancient large igneous province? Geology 25, 299–302.

Heilbron M., Cordani U.C., Alkmim F.F., 2017. The São Francisco Craton and Its Margins. In: M. Cordani, U.G, Heilbron, M., Alkmim, F. F. (eds), São Francisco Craton, Eastern Brazil, Tectonic Genealogy of a Miniature Continent. Regional Geology Reviews, Springer International Publishing Switzerland, pp. 3-13. doi:10.1007/978-3-319-01715-0_1.

Hickman, A.H., 2012. Review of the Pilbara Craton and Fortescue Basin, Western Australia: crustal evolution providing environments for early life. Isl. Arc 21, 1–31.

Jones, D.L., Robertson, I.D.M., McFadden, P.L., 1975. A palaeomagnetic study of Precambrian dyke swarms associated with the Great Dyke of Rhodesia. S. Afr. J. Geol. 78, 57–65.

Kampmann, T.C., Gumsley, A.P., de Kock, M.O., Söderlund, U., 2015. U-Pb geochronology and paleomagnetism of the Westerberg Sill Suite, Kaapvaal Craton - Support for a coherent Kaapvaal-Pilbara Block (Vaalbara) into the Paleoproterozoic? Precambr. Res. 269, 58–72.

Kilian, T., Bleeker, W., Chamberlain, K., Evans, D.A.D., Cousens, B., 2015. Palaeomagnetism, geochronology and geochemistry of the Palaeoproterozoic Rabbit Creek and Powder River dyke swarms: implications for Wyoming in supercraton Superia. In: Li, Z.X., Evans, D.A.D., Murphy, J.B. (eds) Supercontinent Cycles Through Earth History. Geological Society, London, Special Publications, 424, http://doi.org/10.1144/SP424.7.

Kirschvink, J.L., 1980. The least-squares line and plane and the analysis of paleomagnetic data. Geophys. J. R. Astron. Soc. 62, 699–718.

Van Kranendonk, M.J., Altermann, W., Beard, B.L., Hoffman, P.F., Johnson, C.J., Kasting, J.F., Melezhik, V.A., Nutman, A.P., Papineau, D., Pirajno, F., 2012. A chronostratigraphic division of the Precambrian: possibilities and challenges. In: Gradstein, F.M., Ogg, J.G., Schmitz, M.D., Ogg, G.J. (Eds.), The Geologic Time Scale 2012. Elsevier, Boston, USA, pp. 299–392.

Kullerud, K., Skjerlie, K.P., Corfu, F., de la Rosa, J.D., 2006. The 2.40 Ga Ringassøy mafic dikes, West Troms Basement Complex, Norway: the concluding act of Early Palaeoproterozoic continental breakup. Precambr. Res. 150, 183–200.

Krogh, T., 1994. Precise U-Pb ages for Genvillian and pre-Grenvillian thrusting of Proterozoic and Archean metamorphic assemblages in the Grenville Front tectonic zone, Canada. Tectonics 13, 963–982.

Lahtinen, R., Garde, A.A., Melezhik, V.A., 2008. Paleoproterozoic evolution of Fennoscandia and Greenland. Episodes 31, 20–28.

Lubnina, N.V., Slabunov, A.I., 2009. Paleomagnetism in the Neoarchean Polyphase Panozero Intrusion in the Fennoscandian Shield. Mosc. Univ. Geol. Bull. 64, 346–353.

Lubnina, N., Ernst, R., Klausen, M., Söderlund, U., 2010. Paleomagnetic study of NeoArchean-Paleoproterozoic dykes in the Kaapvaal craton. Precambr. Res. 183, 523–552.

Mänttäri, I., Hölttä, P., 2002. U-Pb dating of zircons and monazites from Archean granulites in Varpaisjärvi, central Finland: evidence for multiple metamorphism and Neoarchean terrane accretion. Precambr. Res. 118, 101–131.

Mascarenhas, J.F., Sá, J.H.S., 1982. Geological and metallogenic patterns in the Archean and Early Proterozoic of Bahia State, Eastern Brazil. Revista Brasileira de Geociências 12, 193–214.

McElhinny, M.W., Powell, C. McA, Pisarevsky, S.A., 2003. Paleozoic terranes of eastern Australia and the drift history of Gondwana. Tectonophysics 362, 41–65.

Meert, J.G., Van der Voo, R., Patel, J., 1994. Paleomagnetism of the Late Archean Nyanzian system, western Kenya. Precambr. Res. 69, 113–131.

Meert, J.G., Van der Voo, R., Patel, J., 2016. A Neoarchean paleomagnetic pole from the Kisii Series of western Kenya: implications for crustal mobility. Precambr. Res. 279, 91–102.

Mertanen, S., Korhonen, F., 2011. Paleomagnetic constraints on an Archean-Paleoproterozoic Superior-Karelia connection: New evidence for Archean Karelia. Precambr. Res. 186, 193–204.

Mertanen, S., Halls, H.C., Vuollo, J.I., Pesonen, L.J., Stepanov, V.S., 1999. Paleomagnetism of 2.44 Ga mafic dykes in Russian Karelia, eastern Fennoscandian Shield - implications for continental reconstructions. Precambr. Res. 98, 197–221.

Mertanen, S., Hölttä, P., L.J., Paavola, J., 2006a. Palaeomagnetism of Palaeoproterozoic dolerite dykes in central Finland, Dyke Swarms - Time Markers of Crustal Evolution, ed. Hanski et al. Taylor & Francis, London, book, pp. 243–256.

Mertanen, S., Vuollo, J.I., Huhma, H., Arestova, N.A., Kovalenko, A., 2006b. Early Paleoproterozoic - Archean dykes and gneisses in Russian Karelia of the Fennoscandian Shield - new paleomagnetic, isotope age and geochemical investigations. Precambr. Res. 144, 239–260.

Mitchell, R.N., Evans, D.A.D., Kilian, T.M., 2010. Rapid Early Cambrian rotation of Gondwana. Geology 38, 755–758.

Mushayandebvu, M.F., Jones, D.L., Briden, J.C., 1994. A palaeomagnetic study of the Umvimeela Dyke, Zimbabwe: evidence for a Mesoproterozoic overprint. Precambr. Res. 69, 269–280.

Nemchin, A.A., Pidgeon, R.T., 1998. Precise conventional and SHRIMP baddeleyite U-Pb age for the Binneringie Dyke, near Narrogin, Western Australia. Aust. J. Earth Sci. 45, 673–675.

Noble, S.R., Lightfoot, P.C., 1992. U-Pb baddeleyite ages of the Kerns and Triangle Mountain intrusions, Nipissing Diabase, Ontario. Can. J. Earth Sci. 29, 1424–1429.

Oliveira, E.P., 2011. The Late Archaean Uauá Mafic Dyke Swarm, São Francisco Craton, Brazil, and implications for Palaeoproteozoic extrusion tectonics and orogen reconstruction. In: Srivastava, R.K. (Ed.), Dyke Swarms: Keys for Geodynamic Interpretation. Springer, Berlin, pp. 19–31.

Oliveira, E.P., Lafon, J.M., Souza, Z.S., 1999. Archaean-Proterozoic transition in the Uauá Block, NE São Francisco Craton, Brazil: U-Pb, Pb–Pb and Nd isotope constraints. VII Simpósio Nacional de Estudos Tectônicos, Lençóis, pp. 38–40.

Oliveira, E.P., Mello, E.F., McNaughton, N., 2002. Reconnaissance U-Pb geochronology of early Precambrian quartzites from the Caldeirão belt and their basement, NE São Francisco Craton, Bahia, Brazil: implications for the early evolution of the Palaeoproterozoic Salvador-Curaçá Orogen. J. S. Am. Earth Sci. 15, 349–362.

Oliveira, E.P., McNaughton, N.J., Armstrong, R., 2010. Mesoarchaean to Palaeoproterozoic growth of the northern segment of the Itabuna Salvador Curaçá orogen, São Francisco craton, Brazil. Geological Society, London, Special Publications 338, 263–286. https://doi.org/10.1144/SP338.13.

Oliveira, E.P., Souza, Z.S., McNaughton, N.J., Lafon, J.M., Costa, F.G., Figueiredo, A.M., 2011. The Rio Capim volcanic–plutonic–sedimentary belt, São Francisco Craton, Brazil: Geological, geochemical and isotopic evidence for oceanic arc accretion during Palaeoproterozoic continental collision. Gondwana Res. 19, 735–750.

Oliveira, E.P., Silveira, E.M., Söderlund, U., Ernst, R.E., 2013. U-Pb ages and geochemistry of mafic dyke swarms from the Uauá Block, São Francisco Craton, Brazil: LIPs remnants relevant for Late Archaean break-up of a supercraton. Lithos 174, 308–322.

Oliveira, E.P., McNaughton, N.J., Windley, B.F., Carvalho, M.J., Nascimento, R.S., 2015a. Detrital zircon U-Pb geochronology and whole-rock Nd-isotope constraints on sediment provenance in the Neoproterozoic Sergipano orogen, Brazil: from early passive margins to late foreland basins. Tectonophysics 662, 183–194.

Oliveira E., Amaral W., Talavera C., Semprich J., 2015. Late Mesoarchean high-pressure granulites in the Uauá Block, São Francisco Craton, Brazil. Goldschmidt 2015 Abstracts, p. 2338.

Oliveira, E.P., Amaral, W., Baldin, M.R., Talavera, C., Sombini, G., Semprich, J., McNaughton, N., 2016. The Uauá microblock, northern S. Francisco Craton: A key area to understanding crustal growth during global spread of plate tectonics in the Mesoarchaean. In: Proceedings of the 48th Brazilian Geology Congress, Porto Alegre, Abstract 8445.

Olsson, J.R., Soderlund, U., Klausen, M.B., Ernst, R.E., 2010. U/Pb baddeleyite ages linking major Archean dyke swarms to volcanic rift forming events in the Kaapvaal Craton (South Africa), and a precise age for the Bushveld Complex. Precambr. Res. 183, 490–500.

Paixão, M.A., Oliveira, E.P., 1998. The Lagoa da Vaca Complex: an Archean layered anorthosite body on the western edge of the Uauá Block, Bahia, Brazil. Revista Brasileira de Geociências 28, 201–208.

Pechersky, D.M., Burakov, K.S., Zakharov, V.S., Sharkov, E.V., 2004. Variations in the Geomagnetic Field Direction during Cooling of the Monchegorsk Pluton. Izvestiya Phys. Solid Earth 38, 236–257.

Pidgeon, R.T., 1984. Geochronological constraints on early volcanic evolution of the Pilbara Block, Western Australia. Aust. J. Earth Sci. 31, 237–242.

Pinna, P., Cocherie, A., Thieblemont, D., Jezequel, P., 2000. The Kisii group of western Kenya: an end-Archean (2.53 Ga) late orogenic volcano sedimentary sequence. J. Afr. Earth Sci. 30, 79–97.

Pisarevsky, S.A., de Waele, B., Jones, S., Söderlund, U., Ernst, R.E., 2015. Paleomagnetism and U-Pb age of the 2.4 Ga Erayinia mafic dykes in the south-western Yilgarn, Western Australia: paleogeographic and geodynamic implications. Precambr. Res. 259, 222–231.

Pullaiah, G., Irving, E., 1975. Paleomagnetism of the contact aureole and late dikes of the Otto Stock, Ontario, and its application to Early Proterozoic apparent polar wandering. Can. J. Earth Sci. 12, 1609–1618.

Premo, W.R., Helz, R.T., Zientek, M.L., Langston, R.B., 2000. U-Pb and Sm-Nd ages for the Stillwater Complex and its associated sills and dikes, Beartooth Mountains, Montana: Identification of a parent magma? Geology 18, 1065–1068.

Reddy, S.M., Evans, D.A.D., 2009. Palaeoproterozoic supercontinents and global evolution: Correlations from core to atmosphere. In: Reddy, S.M., Mazumder, R., Evans, D. A.D., Collins, A.S. (eds.) Palaeoproterozoic Supercontinents and Global Evolution. Geological Society of London Special Publications, 323, pp. 1–26.

Salminen, J., Halls, H.C., Mertanen, S., Pesonen, L.J., Vuollo, J., Söderlund, U., 2014. Paleomagnetic and Geochronological Studies on Paleoproterozoic Diabase Dykes of Karelia, East Finland - Key for Testing the Superia Supercraton. Precambr. Res. 22, 87–99. https://doi.org/10.1016/j.precamres.2013.07.011.

Salminen, J., Evans, D.A.D., Trindade, R.I.F., Olivera, E.P., Piispa, E., Smirnov, A., 2016.

Paleogeography of the Congo/São Francisco craton at 1.5 Ga: expanding the core of Nuna supercontinent. Precambr. Res. 286, 195–212.

Schmidt, P.W., Embleton, B.J.J., 1985. Prefolding and overprint magnetic signatures in Precambrian (c.2.9-2.7 Ga) igneous rocks from the Pilbara craton and Hamersley Basin, NW Australia. J. Geophys. Res. 90, 2967–2984.

Selkin, P.A., Gee, J.S., Meurer, W.P., Hemming, S.R., 2008. Paleointensity record from the 2.7 Ga Stillwater Complex, Montana. Geochem. Geophys. Geosyst. 9, Q12023.

Sergeyev, S.A., Lobach-Zhuchenko, S.B., Larionov, A.N., Berezhnaya, N.G., Guseva, N.S., 2007. Archaean age of miaskite lamproites from the Panozero complex, Karelia. Dokl. Earth Sci. 413, 420–423.

Silveira, E.M., Söderlund, U., Oliveira, E., P., Ernst, R.E., and Menez Leal, A.B.,, 2013. First precise U-Pb baddeleyite ages of 1500 Ma mafic dykes from the São Francisco Craton, Brazil, and tectonic implications. Lithos 174, 144–156.

Smirnov, A.V., Evans, D.A.D., Ernst, R.E., Söderlund, U., Li, Z.-X., 2013. Trading partners: Tectonic ancestry of southern Africa and western Australia, in Archean supercratons Vaalbara and Zimgarn. Precambr. Res. 224, 11–22.

Söderlund, U., Hofmann, A., Klausen, M., Olsson, J., Ernst, R., Persson, P.-O., 2010. Towards a complete magmatic barcode for the Zimbabwe craton: baddeleyite U-Pb dating of regional dolerite dyke swarms and sill complexes. Precambr. Res. 183, 388–398.

Strik, G., de Wit, M.J., Langereis, C.G., 2007. Palaeomagnetism of the Neoarchaean Pongola and Ventersdorp Supergroups and an appraisal of the 3.0-1.9 Ga apparent polar wander path of the Kaapvaal Craton, Southern Africa. Precambr. Res. 153, 96–115.

Strik, G., Blake, T.S., Zegers, T.E., White, S.H., Langereis, C.G., 2003. Palaeomagnetism of flood basalts in the Pilbara Craton, Western Australia: Late Archaean continental drift and the oldest known reversal of the geomagnetic field. J. Geophys. Res. 108, 1–21.

Teixeira, W., Figueiredo, M.C.H., 1991. An outline of Early Proterozoic crustal evolution in the São Francisco Craton, Brazil: a review. Precambr. Res. 53, 1–22.

Teixeira, W., Sabaté, P., Barbosa, J., Noce, C.M., Carneiro, M.A., 2000. Archean and Paleoproterozoic tectonic evolution of the São Francisco Craton. In: Cordani, U.G., Milani, E.J., Thomaz Filho, A., Campos, D.A. (Eds.), Tectonic Evolution of South America: 31st International Geological Congress, Rio de Janeiro, pp. 107–137.

Teixeira, W., Oliveira, E.P., Marques, L.S., 2017. Nature and evolution of the Archean crust of the São Francisco Craton: a review. In: Cordani, U.G., Heilbron, M., Alkmim, F.F. (Eds.), São Francisco Craton, Eastern Brazil. Tectonic Genealogy of a Miniature Continent. Regional Geology Reviews, Springer International Publishing, pp. 29–56.

Trendall, A.F., 1968. Three great basins of Precambrian iron formation deposition: a systematic comparison. Geol. Soc. Am. Bull. 79, 1527–1533.

Trindade, R.I.F., D'Agrella-Filho, M.S., Babinsky, M., Font, E., Brito Neves, B.B., 2004. Paleomagnetism and geochronology of the Bebedouro cap carbonate: evidence for continental-scale Cambrian remagnetization in the São Francisco craton, Brazil. Precambr. Res. 128, 83–103.

Yoshihara, A., Hamano, Y., 2004. Paleomagnetic constraints on the Archean geomagnetic field intensity obtained from komatiites of the Barberton and Belingwe greenstone belts, South Africa and Zimbabwe. Precambr. Res. 131, 111–142.

Van der Voo, R., 1990. The reliability of paleomagnetic data. Tectonophysics 184, 1–9.

Vuollo, J., Huhma, H., 2005. Paleoproterozoic mafic dykes in NE Finland. In: Lehtinen, M., Nurmi, P.A., Rämö, O.T. (Eds.), Precambrian Geology of Finland—Key to the Evolution of the Fennoscandian Shield. Elsevier Science B.V, Amsterdam, pp. 195–236.

Williams, H., Hoffman, P.F., Lewry, J.F., Monger, J.W.H., Rivers, T., 1991. Anatomy of North America: thematic geologic portrayals of the continent. Tectonophysics 187, 117–134.

Wingate, M.T.D., 1998. A palaeomagnetic test of the Kaapvaal - Pilbara (Vaalbara) connection at 2.78 Ga. S. Afr. J. Geol. 101, 257–274.

Wingate, M.T.D., 1999. Ion microprobe baddeleyite and zircon ages for late Archean mafic dykes of the Pilbara Craton, Western Australia. Aust. J. Earth Sci. 46, 493–500.

Wingate, M.T.D., 2000. Ion microprobe U—Pb zircon and baddeleyite ages for the Great Dyke and its satellite dykes, Zimbabwe. S. Afr. J. Geol. 103, 74–80. https://doi.org/10.2113/103.1.74.